

<https://doi.org/10.1038/s42003-024-07342-8>

Protogenin facilitates trunk-to-tail *HOX* code transition via modulating GDF11/SMAD2 signaling in mammalian embryos

Check for updates

Yu-Sheng Hung¹, Wei-Mi Lin^{1,2,5}, Yu-Chiuan Wang^{3,5}, Wei-Chih Kuo^{1,5}, Yu-Yang Chen⁴, Ming-Ji Fann^{1,3,4}, Jenn-Yah Yu^{1,2,4} & Yu-Hui Wong ^{1,2,3,4}

During embryogenesis, vertebral axial patterning is intricately regulated by multiple signaling networks. This study elucidates the role of protogenin (*Prtg*), an immunoglobulin superfamily member, in vertebral patterning control. *Prtg* knockout (*Prtg*^{-/-}) mice manifest anterior homeotic transformations in their vertebral columns and significant alterations in homeobox (*Hox*) gene expression. Transcriptomic profiling of *Prtg*^{-/-} mouse embryos highlights *Prtg*-regulated genes involved in axial development, particularly within the transforming growth factor beta (TGF β) signaling pathway. Reduced TGF β signaling in *Prtg*^{-/-} mouse embryos is evidenced by decreased phosphorylated Smad2 (pSmad2) levels and its downstream target genes in the developing tail. We further show that *Prtg* interacts with growth differentiation factor 11 (GDF11) to enhance GDF11/pSmad2 signaling activity. Using human-induced pluripotent stem cell-derived presomitic mesoderm-like (hiPSC-PSM) cells, we demonstrate delayed posterior *HOX* gene expression upon *PRTG* knockout, which is rescued by GDF11 supplementation. These findings provide compelling evidence that *PRTG* regulates *HOX* genes through the GDF11/SMAD2 signaling pathway.

The vertebral column is one of the most distinctive features of vertebrate animals. It comprises a series of spinal elements with specific morphological characteristics. Based on their morphology, these elements are categorized into cervical, thoracic, lumbar, sacral, and caudal sections¹. In humans, the vertebral column consists of 33 bones, including 7 cervical, 12 thoracic, 5 lumbar, and 5 sacral vertebrae, as well as 4 caudal bones that fuse to form the coccyx. Mice possess 7 cervical, 13 thoracic, 6 lumbar, 4 sacral, and more than 10 caudal vertebrae. These bony elements arranged along the anterior-posterior axis constitute the axial patterning of the vertebral column.

Vertebral axial patterning is established during embryogenesis. After the formation of three germ layers, a group of cells located at the caudal end of the embryo, namely, neuromesodermal progenitors (NMPs), continues to generate daughter cells that contribute to both ectodermal and mesodermal lineages²⁻⁴. The mesodermal lineage includes presomitic mesodermal (PSM) cells that further proliferate and differentiate to form somites. This process is called somitogenesis⁵. Since vertebral bones are derived from somites⁶, the positional identity of each somite, which is determined based on homeobox (*Hox*) gene expression, contributes to the morphological characteristics of each vertebra⁷.

Hox proteins belong to a large family of transcriptional factors containing the homeobox DNA binding domain⁸. Both human and mouse genomes contain 39 *Hox* genes divided into four clusters: *Hoxa*, *Hoxb*, *Hoxc*, and *Hoxd*. Within each cluster, *Hox* genes are further divided into 13 paralogs, designated *Hox1* to *Hox13*⁷. During somitogenesis, *Hox* genes are activated in a temporally collinear sequence, where low-numbered *Hox* genes are activated first to specify future anterior vertebrae, while their high-numbered counterparts are activated later to establish future posterior vertebrae. For example, *Hox4* and *Hox5* define the cervical vertebrae, *Hox6* defines the anterior thoracic containing ribs attached to the sternum, and *Hox9* defines the posterior thoracic containing ribs not attached to the sternum⁹⁻¹¹. The transition from thoracic to lumbar identity is defined by *Hox10* expression, while *Hox11* expression corresponds to the sacral and caudal vertebrae¹².

The expression of *Hox* genes is regulated by multiple signaling pathways. During gastrulation, activation of the Wnt signaling in NMPs induces the expression of anterior *Hox* genes *Hox1* to *Hox5*¹³, which define the cervical and anterior thoracic vertebrae. The Wnt signaling

¹Department of Life Sciences and Institute of Genome Sciences, College of Life Sciences, National Yang Ming Chiao Tung University, Taipei, Taiwan (ROC).

²Interdisciplinary Master Program in Molecular Medicine, College of Life Sciences, National Yang Ming Chiao Tung University, Taipei, Taiwan (ROC). ³Institute of Neuroscience, College of Life Sciences, National Yang Ming Chiao Tung University, Taipei, Taiwan (ROC). ⁴Brain Research Center, National Yang Ming Chiao Tung University, Taipei, Taiwan (ROC). ⁵These authors contributed equally: Wei-Mi Lin, Yu-Chiuan Wang, Wei-Chih Kuo. e-mail: jyyu@nycu.edu.tw;

yuhui.wong@nycu.edu.tw

further activates its downstream target gene caudal type homeobox 2 (*Cdx2*), which encodes a homeobox transcription factor inducing the expression of trunk *Hox* genes (*Hox6* to *Hox9*)^{14,15} corresponding to the identities of posterior thoracic vertebrae. Thereafter, growth differentiation factor 11 (*Gdf11*), a member of the transforming growth factor-beta (*TGFβ*) family, induces the activation of posterior *Hox* genes (*Hox10* to *Hox13*) to specify lumbar, sacral, and caudal vertebrae identities^{16–18}. This sequential activation of *Hox* genes establishes the axial patterning of vertebrae.

The *TGFβ* signaling has been reported to play important roles in embryogenesis and tissue homeostasis. Both human and mouse genomes encode 33 *TGF-β* family ligands, including *GDF11*. The *TGF-β* ligand is first translated as a propeptide, which is processed into a mature polypeptide¹⁹. Activation of the *TGFβ* signaling involves the binding of *TGFβ* ligands to form a heteromeric complex comprising the mature ligand dimer and two pairs of *TGFβ* type I and type II receptors²⁰. This ligand-receptor complex triggers the phosphorylation of receptor-related Smads, *Smad2* and *Smad3*. Phosphorylated *Smad2/3* forms a heterotrimer with the co-Smad, *Smad4*, and translocates into the nucleus to regulate the expression of target genes. Several studies have demonstrated the role of *Gdf11* in the development of posterior vertebrae. In *Gdf11* signaling-deficient mice, abnormal tail development and homeotic transformation are associated with impaired activation of caudal *Hox* genes^{16,17,21,22}. The *cis*-regulatory elements within the *Hox* loci contain *Smad*-binding motifs that respond to *Gdf11*^{23,24}. In addition, *GDF11* administration efficiently activates the expression of *HOX10* and more posterior *HOX* genes in neurons or mesodermal cells derived from human embryonic stem cells or induced pluripotent stem cells (hiPSCs)^{25,26}. Thus, the *GDF11/SMAD2* signaling pathway plays a key role in activating posterior *HOX* genes to induce the trunk-to-tail *HOX* code transition and promote caudal development. However, regulators mediating the *GDF11* signaling activity remain largely unexplored.

Protogenin (*Prtg*), also known as *Igdcc5*, encodes a single-pass transmembrane protein belonging to the immunoglobulin superfamily (IgSF). *Prtg* is the fifth member of the deleted colorectal carcinoma (DCC) subclass containing four immunoglobulin domains and five fibronectin type III domains in its extracellular portion²⁷. During mouse embryogenesis, *Prtg* is abundantly expressed in the neural tube and mesodermal cells between embryonic days 8 (E8) and 10 (E10) and down-regulated after E10.5^{28,29}. *Prtg* signaling has been shown to suppress premature neuronal differentiation during the early stages of neural development²⁸. *Prtg* also participates in tooth germ development and differentiation of inner enamel epithelial cells³⁰. In addition, it modulates apoptosis and migration of rostral cephalic neural crest cells³¹. Recent studies have identified early rhombic lip PRTG-positive stem cells within a human-specific neurovascular niche as critical initiators and maintainers of group 3 medulloblastoma, further highlighting the significance of PRTG in both normal development and pathological conditions³². Despite its prolific expression in the developing mesoderm, the function of *Prtg* in somitogenesis is yet to be elucidated.

In this study, we demonstrated the roles of *Prtg* using mice harboring a conventional knockout allele of *Prtg* (*Prtg*^{-/-})³¹. *Prtg*^{-/-} mice exhibited a robust phenotype of anterior homeotic transformation in the thoracic vertebrae accompanied by altered expression patterns of thoracic- and lumbar-associated *Hox* genes. Based on transcriptional profiles and whole-mount staining, we revealed that the *TGFβ* signaling is significantly down-regulated in the posterior region of E9.5 *Prtg*^{-/-} embryos. In addition, we demonstrated that *Prtg* interacts with *Gdf11* and enhances the *Gdf11/pSmad2* signaling activity. To verify our findings, we developed a novel hiPSC-derived PSM-like (hiPSC-PSM) model that enabled us to accurately reconstitute the delayed expression of posterior *Hox* genes observed in *Prtg*^{-/-} mice. Importantly, this delayed expression of posterior *HOX* genes could be effectively reversed by *GDF11* administration, suggesting that PRTG regulates *HOX* gene expression via the *GDF11/SMAD2* signaling.

Results

Anterior homeotic transformation of thoracic vertebrae in *Prtg*-deficient mice

Prtg exhibits unique spatiotemporal changes in expression during early embryonic development in mice^{28,29}. At embryonic day 9.5 (E9.5), *Prtg* is ubiquitously expressed throughout the body axis. Subsequently, its expression diminishes from head to tail from E10.5 to E11.5. To investigate the potential role underlying the dynamic expression pattern of *Prtg*, we have previously generated conventional *Prtg* knockout (*Prtg*^{-/-}) mice and reported the associated defects in palatine and skull development³¹. In addition, we identified significant defects in the vertebral patterning of *Prtg*^{-/-} mice (Fig. 1a). In *Prtg*^{-/-} neonatal mice, the number of sternum-attached ribs increased from 7 to 10, compared with wild-type (WT) control mice. The number of rib-bearing vertebrae increased from 13 to 15, whereas those of cervical and lumbar vertebrae remained constant. Moreover, the posterior thoracic vertebrae (T8–T15) in *Prtg*^{-/-} mice adopted shapes resembling those of anterior thoracic vertebrae (Fig. 1b), suggesting an anterior transformation phenotype. This anterior transformation was observed in 96% of *Prtg*^{-/-} mice, but not in WT or *Prtg* heterozygous mice (*Prtg*^{+/-}) (Table 1), and was consistent across different genetic backgrounds (Supplementary Table 1). The number and shape of lumbar vertebrae in *Prtg*^{-/-} mice were comparable to those in the control mice. To determine whether the additional rib-bearing vertebrae resulted from an increase in somite number, we analyzed somite formation in E11 embryos using *in situ* hybridization of myogenin (*Myog*), a marker of differentiated somites. The total number of *Myog*-positive somites in control and *Prtg*^{-/-} embryos was consistent, ranging from 29 to 33 somites. However, we observed a posterior displacement of two somites in the anterior boundary of hindlimb buds in *Prtg*^{-/-} embryos, transitioning from the 24th to the 26th *Myog*-expression domains (Fig. 1c, d and Supplementary Table 2). These findings highlight the critical role of *Prtg* in the specification of vertebrae along the anterior-posterior axis.

Hox gene expression is dysregulated in *Prtg*^{-/-} embryos

Vertebral morphologies and characteristics are determined by the spatial and temporal expression of *Hox* genes⁷. It is possible that *Prtg* regulates the specification of thoracic vertebrae by modulating *Hox* gene expression. To explore this hypothesis, we examined *Hox* gene expression at E10.5, shortly after somite generation occurs in the posterior thoracic-to-lumbar region during development (Fig. 1e). In *Prtg*^{-/-} embryos, the expression levels of *Hox* genes associated with cervical and thoracic identity were elevated. Specifically, *Hoxc8* expression was increased, while *Hoxb6* and *Hoxb9* displayed both increased and posteriorly extended-expression patterns. Conversely, *Prtg*^{-/-} embryos showed a decreased expression of lumbar-associated *Hox* genes; *Hoxa10* was down-regulated, and expression patterns of *Hoxc9* and *Hoxd9* shifted posteriorly. *Hoxc10* and *Hoxd10* exhibited both decreased and posteriorly shifted expression patterns in *Prtg*^{-/-} embryos. Importantly, abnormal expressions of *Hox* genes in *Prtg*^{-/-} mice corresponded to the thoracic vertebrae transformation phenotype. These results indicate a potential role of *Hox* genes in mediating the anterior homeotic transformation phenotypes in *Prtg*^{-/-} mice (Fig. 1f).

Prtg regulates genes associated with the development of the body axis

Abnormal vertebrae in *Prtg*^{-/-} mice develop from the 19th to the 27th somite (Fig. 1f), which are formed between E9 and E10. To elucidate the molecular basis underlying the anterior homeotic transformation of vertebrae in *Prtg*^{-/-} embryos, we conducted mRNA sequencing (mRNA-seq) analysis wherein *Prtg*^{+/+} (WT), *Prtg*^{+/-}, and *Prtg*^{-/-} embryos were compared with one another. The posterior trunk after the forelimb bud (13th somite) of E9.5 embryos was dissected for mRNA-seq to enrich genes expressed in the thoracic somites (Fig. 2a). The mRNA profiles of WT and *Prtg*^{+/-} embryos were similar, as only six differentially expressed genes (DEGs) were observed, thus explaining the normal vertebral pattern in *Prtg*^{+/-} mice (Fig. 2b and Supplementary Fig. 2). To be convenient, *Prtg*^{+/+} (WT) and *Prtg*^{+/-} embryos were combined as the control group for subsequent analyzes. Transcriptomic profiling revealed 529

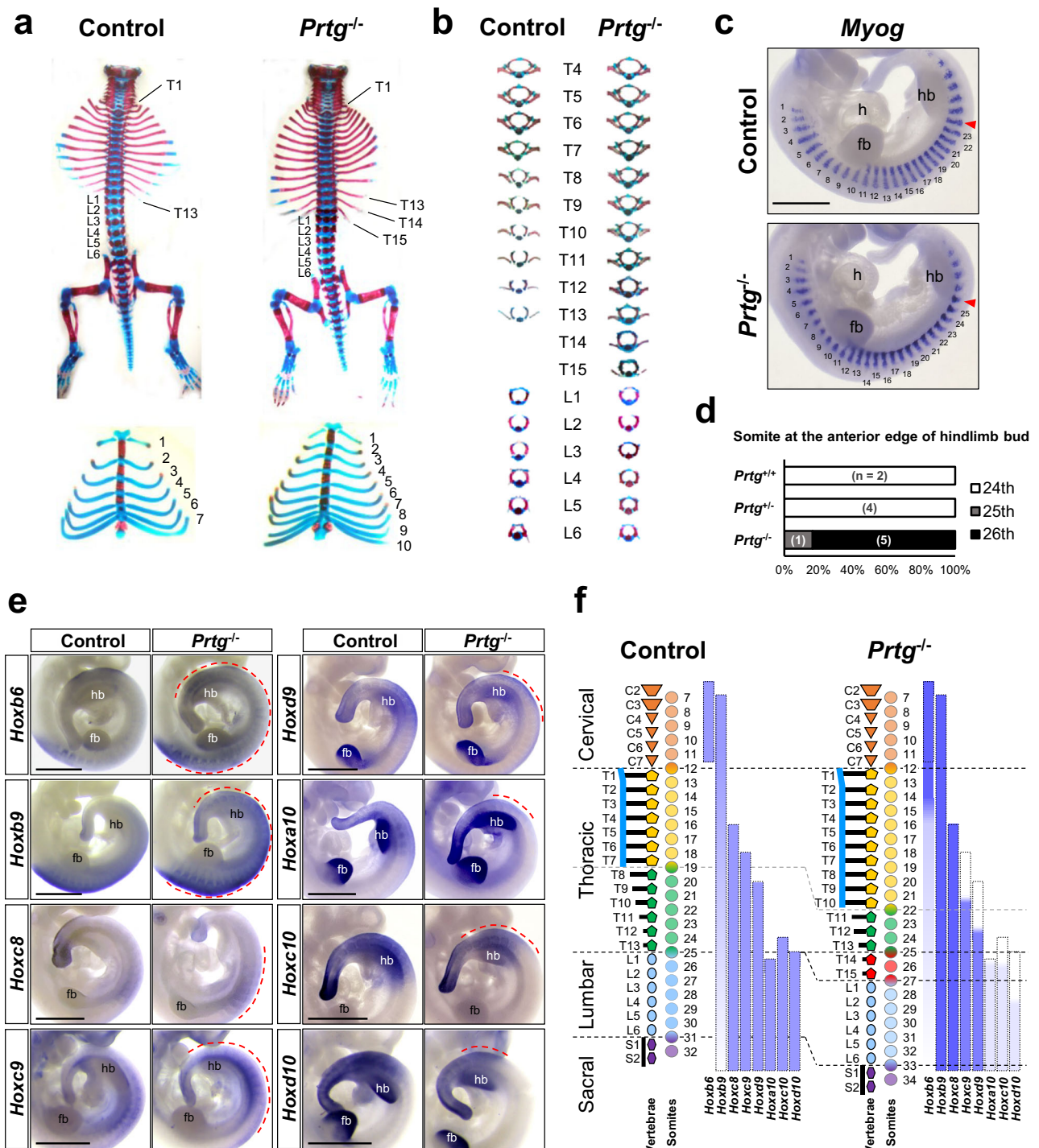


Fig. 1 | Anterior homeotic transformation in the vertebrae of *Prtg*^{-/-} mice. **a** Skeletal and cartilaginous tissue staining of control and *Prtg*^{-/-} neonatal mice. Two additional thoracic vertebrae (top) and three more sternum-attached rib pairs (bottom) were observed in *Prtg*^{-/-} mice. **b** Isolated thoracic and lumbar vertebrae from control and *Prtg*^{-/-} mice. In *Prtg*^{-/-} mice, T8 to T10 were transformed into a T7-like shape, while T11 to T13 were transformed into a T8-like shape ($n = 32$). **c** Whole-mount in situ hybridization of *Myog* mRNA in E11.0 control and *Prtg*^{-/-} embryos. The somite at the anterior edge of the hindlimb bud is indicated by a red arrowhead. The scale bar represents 1 mm; fb forelimb bud, h heart, hb hindlimb bud. **d** Quantification results of the somite number located at the anterior edge of the hindlimb bud, which has been visualized and manually enumerated as shown in (c), in E11.0 *Prtg*^{+/+} ($n = 2$), *Prtg*^{+/-} ($n = 4$), and *Prtg*^{-/-} ($n = 6$) embryos from 2 litters.

e Whole-mount in situ hybridization of *Hoxb6* ($n = 10$), *Hoxb9* ($n = 10$), *Hoxc8* ($n = 5$), *Hoxc9* ($n = 8$), *Hoxd9* ($n = 5$), *Hoxa10* ($n = 5$), *Hoxc10* ($n = 4$), and *Hoxd10* ($n = 4$) in control and *Prtg*^{-/-} embryos. In situ hybridization of *Hoxa10* was performed on E11.0 and that of others on E10.0. Dashed red lines indicate the regions where *Prtg*^{-/-} embryos displayed differential expression compared with control embryos. Scale bars represent 1 mm. **f** Summary of the vertebral phenotypes and *Hox* expression patterns in control and *Prtg*^{-/-} mice. Dashed boxes delineate the regions of *Hox* gene expression in the control group. The intensity of the blue color indicates the level of *Hox* gene expression observed by in situ hybridization. C cervical vertebra (orange), L lumbar vertebra (light blue), S sacral vertebra (purple), T thoracic vertebra (yellow and green). Red-colored vertebrae indicate additional vertebrae in *Prtg*^{-/-} mice.

Table 1 | Penetrance of vertebral defects in *Prtg* mutants

Type of transformation	Transformed ribs					Other transformation				
	T1 to C7	T2 to T1	T8 to T7	L1 to T13	L2 to T13	L3 to T13	T8-T10 = T7	T11-T13 = T8	S2 to L6	
Description	Abnormal T1 rib	Abnormal T2 rib	8th rib at sternum	14th rib on L1 (T14)	15th rib on L2 (T15)	16th rib on L3 (T16)	T8-T10 vertebrae display a T7-like shape	T11-T13 vertebrae display a T8-like shape	Hindlimb on original S3	
Wild type (n = 27)	0%	0%	0%	0%	0%	0%	0%	0%	0%	
<i>Prtg</i> ^{-/-} (n = 32)	16% (3%) [#]	0% (0%) [#]	96% (90%) [#]	96% (96%) [#]	96% (71%) [#]	19% (9%) [#]	96%	96%	96%	

C cervical, L lumbar, S sacral, T thoracic.

[#]The percentage of animals with the bilateral presence of phenotypes is indicated within parentheses.

DEGs, including 267 and 262 up-regulated and down-regulated genes, respectively, in *Prtg*^{-/-} embryos compared with those in the control group (Fig. 2c and Supplementary Data 1). We further used ingenuity pathway analysis (IPA) to analyze DEGs associated with various signaling pathways, diseases, and physiological functions. The DEGs were significantly associated with axial development and skeleton patterning (Fig. 2d), demonstrating that *Prtg* plays an essential role in the specification of vertebrae along the anterior-posterior body axis.

The anterior homeotic transformation phenotypes of *Prtg*^{-/-} embryos suggest that *Prtg* modulates vertebral patterning through *Hox* genes. Indeed, trunk *Hox* genes were up-regulated in the *Hoxb* cluster (*Hoxb7*, *b8*, and *b9*), whereas posterior *Hox* genes (*Hox10-13*) in all four clusters were down-regulated (Fig. 2e). To verify our RNA-seq data, we examined *Hox* gene expression via reverse transcription-quantitative polymerase chain reaction (RT-qPCR) analysis. Consistently, we noted increased trunk *Hox* expression (*Hoxb6-Hoxb9*) and decreased posterior *Hox* expression (*Hoxc9-Hoxc10*) in the posterior region of *Prtg*^{-/-} embryos (Fig. 2f). Taken together, these results suggest that the vertebral transformation in *Prtg*^{-/-} mice is caused by the down-regulation of posterior *Hox* genes (paralogous groups 10-13) along with the up-regulation and posterior shift of trunk *Hox* genes (*b6-b9*).

The TGFβ signaling is down-regulated in *Prtg*^{-/-} embryos

To elucidate molecular mechanisms underlying *Hox* gene regulation by *Prtg*, DEGs between *Prtg*^{-/-} and control embryos were subjected to IPA analysis to identify potential upstream regulators. Predicted upstream regulators included signaling pathways related to the TGFβ (TGFB1) and WNT/β-catenin (CTNNB1) signaling pathways, GTPase regulation (HRAS), SOX2 transcription factor, inflammatory responses (NFKBIA and TNF), and apoptosis (TP53 and TP73) (Fig. 3a). Thereafter, we performed gene set enrichment analysis (GSEA) to investigate signaling pathways regulated by *Prtg*. Among all the pathways examined, the TGFβ pathway exhibited the most significant alteration in *Prtg*^{-/-} embryos (normalized enrichment score [NES] = 1.82, nominal *p*-value = 0, false discovery rate [FDR] *q*-value = 0.014) (Fig. 3b and Supplementary Table 3). Considering the crucial role of the TGFβ signaling in the activation of posterior *Hox* genes, we hypothesized that *Prtg* promotes TGFβ signaling activity to regulate *Hox* gene expression. GSEA results revealed down-regulation of the TGFβ signaling pathway in *Prtg*^{-/-} embryos, characterized by decreased expression of core components, such as *Skil*, *Ski*, *Smad7*, and *Smurf1* (Fig. 3c and Supplementary Table 4). This result was further validated by using RT-qPCR. Expressions of *Skil*, *Smad7*, and *Smurf1* in the posterior trunks of *Prtg*^{-/-} embryos were significantly decreased compared with those of the control (Fig. 3d). This result provides evidence for down-regulation of the TGFβ signaling activity in the posterior trunk of *Prtg*^{-/-} embryos.

Activation of the TGFβ signaling leads to phosphorylation and activation of downstream signaling transducers, Smad2 and Smad3³³. Thus, we examined the TGFβ signaling activity by using western blot analysis and quantifying the ratio of phosphorylated Smad2 (pSmad2) to total Smad2. In the posterior trunk of E9.5 *Prtg*^{-/-} embryos, the pSmad2 ratio was significantly decreased compared with that in the control (Fig. 3e, f). The level of Smad4, a co-Smad involved in both TGFβ and bone morphogenetic protein (BMP) signaling, remained constant. In addition, no obvious change in the expression of those TGFβ ligands, receptors, and Smads was observed in *Prtg*^{-/-} embryos (Supplementary Fig. 3a and Supplementary Table 5). These results indicate that *Prtg* deficiency leads to a down-regulation of the TGFβ signaling activity and a reduction in pSmad2 levels.

A decrease of TGFβ signaling activity in the PSM of *Prtg*^{-/-} embryos

Numerous studies have reported roles of the TGFβ signaling in embryogenesis, including germ layer specification, left-right asymmetry, and axial patterning^{21,34-36}. Since the phenotype of *Prtg*^{-/-} mice manifest in the vertebral column, we examined whether the TGFβ signaling is down-regulated in the posterior mesoderm of *Prtg*^{-/-} mice. We performed whole-mount immunostaining of pSmad2 as an indication of TGFβ signaling activity in

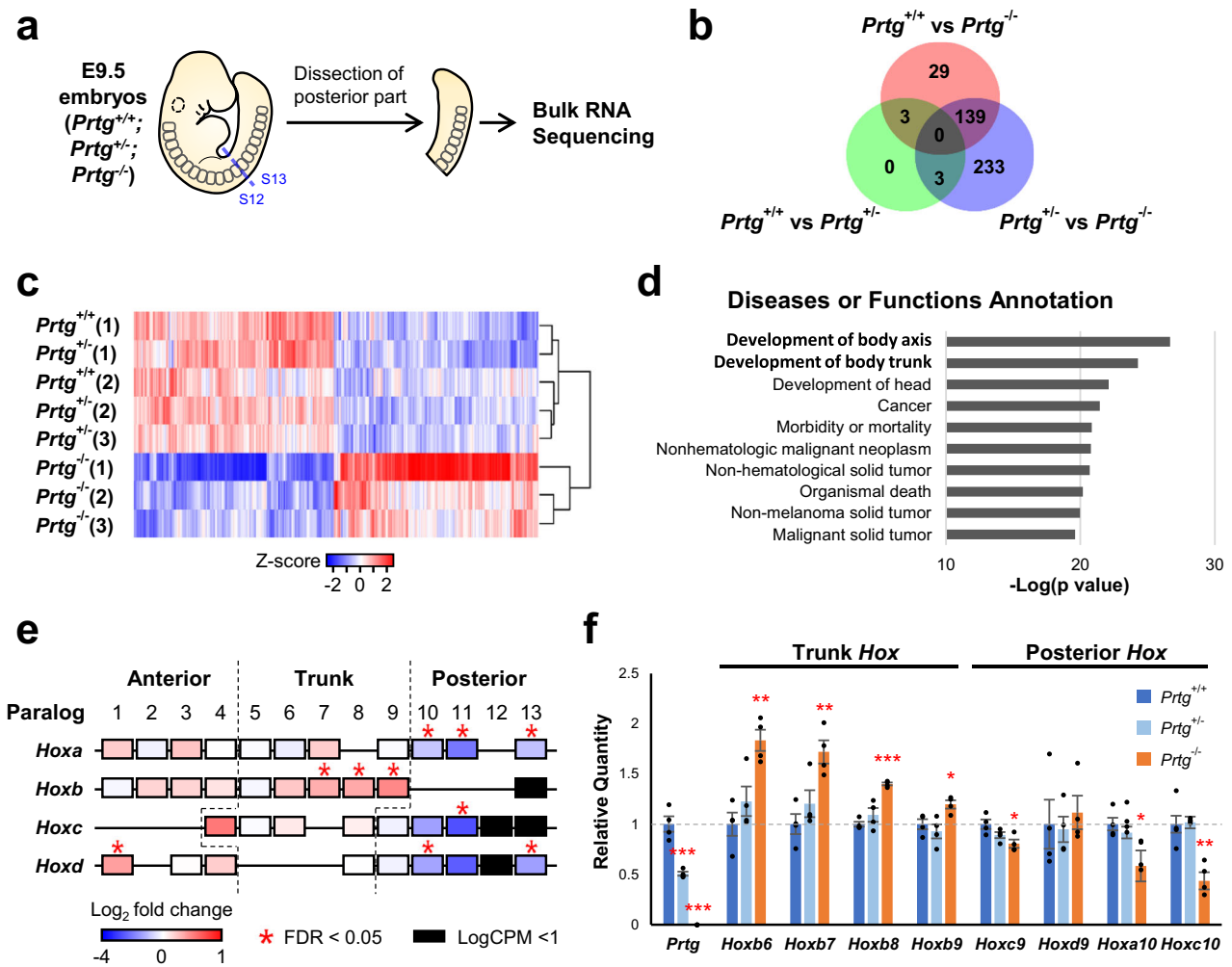


Fig. 2 | Transcriptome analysis of the posterior trunks of E9.5 *Prtg*^{-/-} embryos. **a** Schematic representation of the experimental design for transcriptome analysis. E9.5 embryos were dissected between the 12th and 13th somite, and the posterior trunks were subjected to bulk RNA-seq analysis. **b** Numbers of differentially expressed genes (DEGs) observed in *Prtg*^{+/+} vs *Prtg*^{+/-}, *Prtg*^{+/+} vs *Prtg*^{-/-}, and *Prtg*^{+/-} vs *Prtg*^{-/-} embryos. DEGs were identified using edgeR with FDR < 0.05 as the cutoff. **c** Heatmap of DEGs in the *Prtg*^{+/+}, *Prtg*^{+/-} and *Prtg*^{-/-} samples. A total of 529 DEGs were identified between the control (*Prtg*^{+/+} and *Prtg*^{+/-}) and *Prtg*^{-/-} samples, among which 267 and 262 genes were up-regulated and down-regulated in the *Prtg*^{-/-} samples, respectively. **d** Diseases or

Functions Annotation generated via Ingenuity Pathway Analysis (IPA) illustrating the significant association of *Prtg*-regulated genes with body axis development. **e** Heatmap illustrating the fold change in *Hox* gene expression observed in *Prtg*^{-/-} samples relative to control embryos (*Prtg*^{+/+} and *Prtg*^{+/-}), derived from RNA-seq data. **f** The expression levels of *Prtg*, *Hoxb6*, *Hoxb7*, *Hoxb8*, *Hoxb9*, *Hoxc9*, *Hoxd9*, *Hoxa10*, and *Hoxc10* in the posterior trunk samples of *Prtg*^{+/+}, *Prtg*^{+/-} and *Prtg*^{-/-} embryos were quantified using RT-qPCR. *Tbp* was used as the reference gene. Data are presented as the mean ± SEM. Statistical significance relative to *Prtg*^{+/+} is indicated (*n* = 4 for each bar; **p* < 0.05; ***p* < 0.01; ****p* < 0.001, by one-way ANOVA).

E9.5 embryos (Fig. 4a and Supplementary Movies 1 and 2). In the control embryos, pSmad2 signaling was detected in the tail region and a portion of the heart. In *Prtg*^{-/-} embryos, pSmad2 staining was significantly decreased in the tail region, including the tail bud, presomitic mesoderm (PSM), lateral plate mesoderm (LPM), and neural tube, while remaining unchanged in the heart. Conversely, total Smad2/3 staining was uniformly distributed throughout the body and did not display an obvious difference between the control and *Prtg*^{-/-} embryos (Supplementary Fig. 3b). These results indicate that loss of *Prtg* leads to down-regulation of TGFβ signaling activity in the tail. Furthermore, we verified the expression of genes downstream of the TGFβ pathway by using whole-mount in situ hybridization. The expression levels of *Ski*, *Skil*, and *Smurf1* were reduced in the tail bud and PSM of *Prtg*^{-/-} embryos (Fig. 4c–e and Supplementary Fig. 4b). Interestingly, mesodermal development markers, such as *Cyp26a1*, *T*, *Tbx6* and *Msgn1*, were similar between the control and *Prtg*^{-/-} embryos (Supplementary Fig. 4a), suggesting that down-regulation of TGFβ signaling activity in *Prtg*^{-/-} embryos do not affect mesodermal development. We also compared *Hoxc10* and *Hoxd10* expression in E9.5 embryos by using whole-mount staining followed by sectioning (Fig. 4b, f, g and Supplementary Movies 3 and 4). In the

paraxial mesoderm, the expression of both *Hoxc10* and *Hoxd10* was predominantly in the tail bud and PSM (Fig. 4f, g, left panels). In *Prtg*^{-/-} embryos, *Hoxc10* and *Hoxd10* expression was posteriorly restricted. In sections of the posterior region, expression levels of *Hoxc10* and *Hoxd10* were similar in the tail bud region but dramatically decreased in the PSM region of *Prtg*^{-/-} embryos (Fig. 4f, g, right panels). Collectively, our findings suggest that *Prtg* regulates TGFβ signaling activity in the developing PSM, which is critical for proper expression of posterior *Hox* genes.

Prtg interacts with Gdf11 and modulates its signaling activity

We observed a reduction in pSmad2 levels in the tails of *Prtg*^{-/-} embryos (Fig. 4), which corresponds with the expression pattern of *Gdf11*³⁷. In contrast, the pSmad2 levels in the heart of *Prtg*^{-/-} embryos remained unchanged, where the TGFβ signaling is mediated by *Tgfb1* and *Tgfb2*³⁸. Moreover, it is well established that *Gdf11* regulates posterior *Hox* genes, which were similarly affected in *Prtg*^{-/-} embryos^{16,39}. Our RNA-seq results also revealed a decrease in *Isl1* expression and a slight increase in *Lin28* expression (Supplementary Data 1), indicating a down-regulation of *Gdf11*

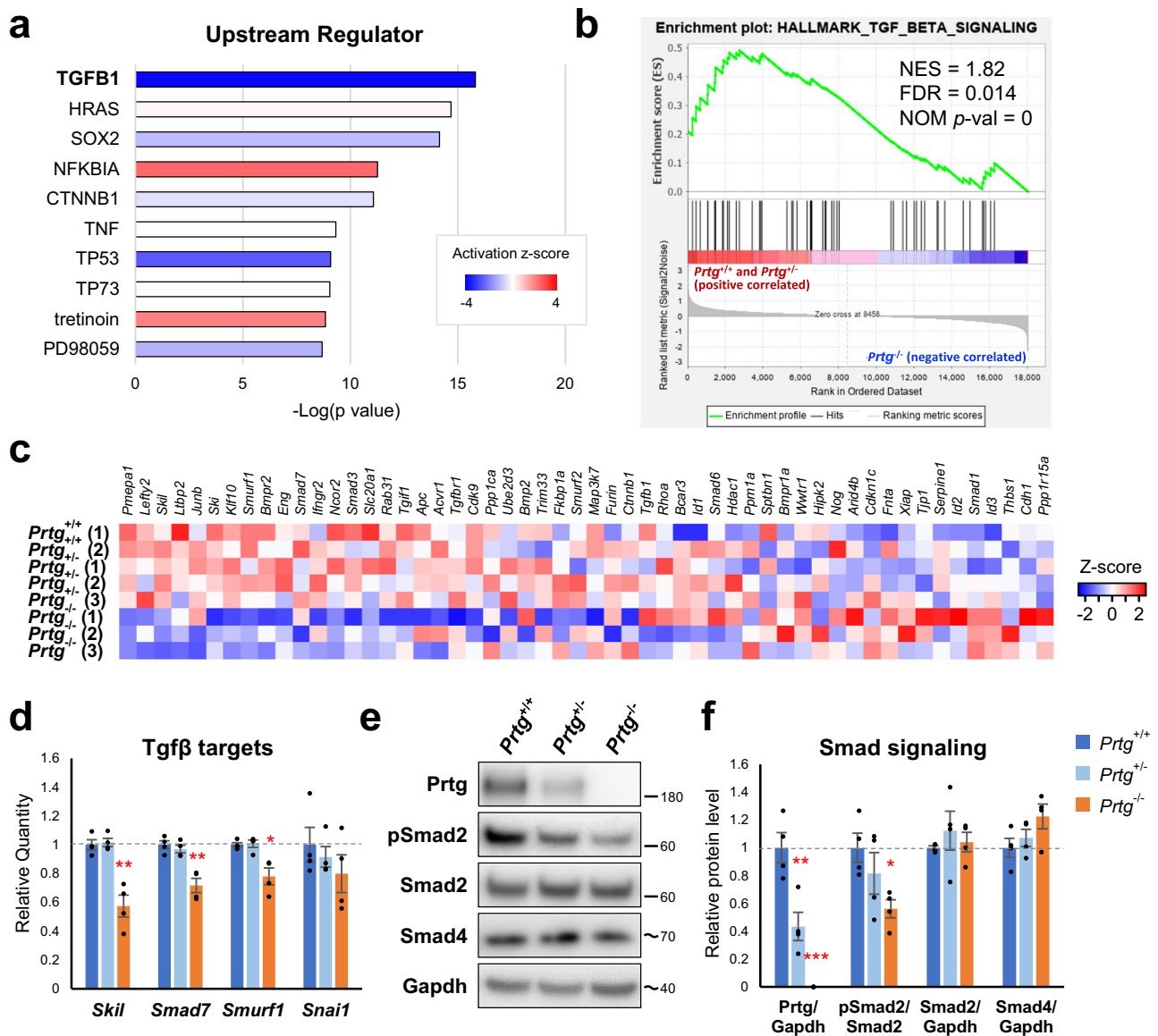


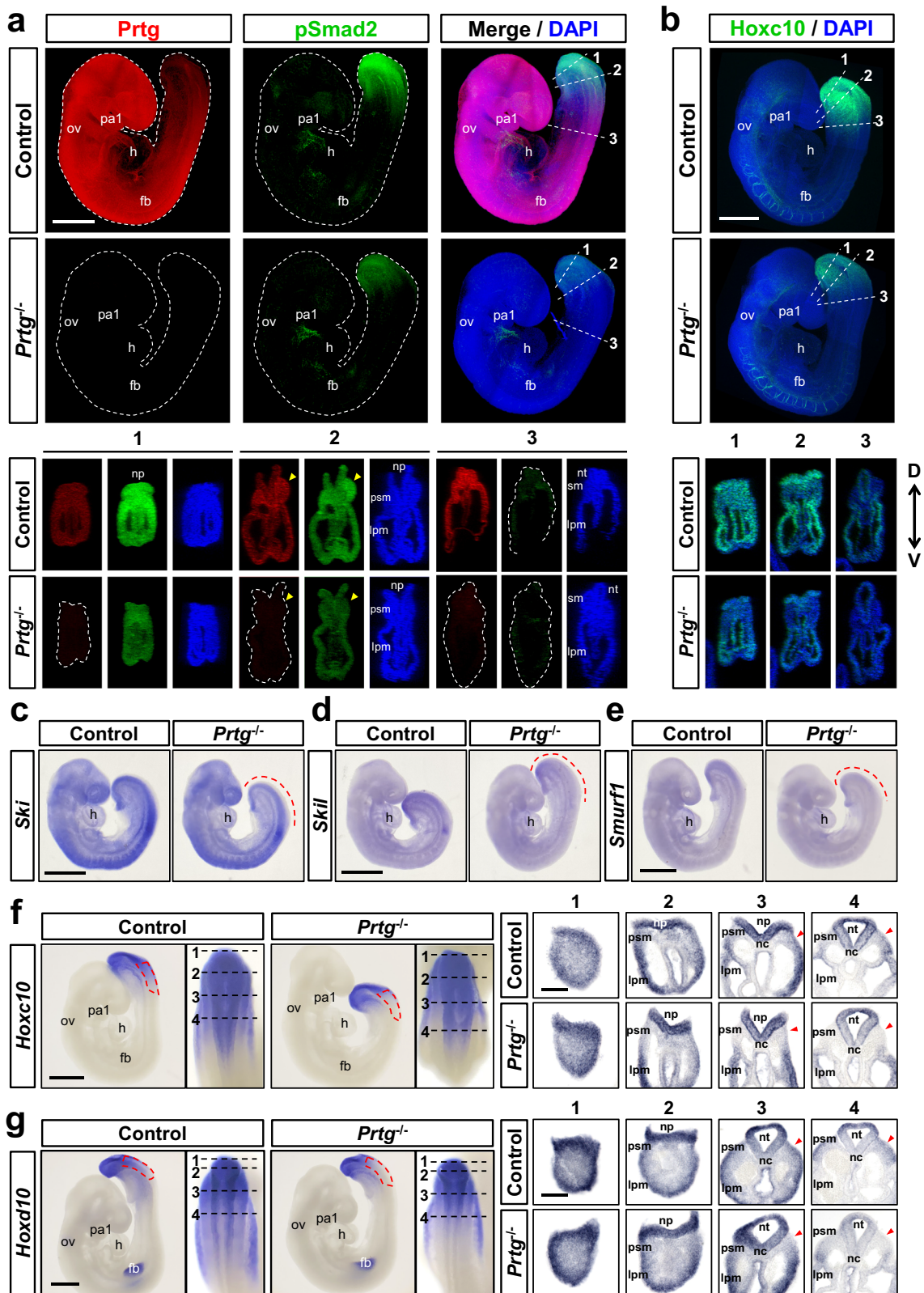
Fig. 3 | Down-regulation of TGFβ signaling activity in the posterior trunks of E9.5 *Prtg*^{-/-} embryos. **a** Upstream regulator analysis via IPA demonstrated that the DEGs in the *Prtg*^{-/-} samples were significantly associated with TGFβ1. **b** GSEA revealed that TGFβ signaling was significantly altered in *Prtg*^{-/-} embryos. **c** Heatmap of the expression levels of genes within the TGFβ signaling gene set. **d** The expression levels of TGFβ signaling target genes in the *Prtg*^{+/+}, *Prtg*^{+/-}, and *Prtg*^{-/-} posterior trunk samples were quantified using qRT-PCR. *Tbp* was used as the reference gene. Data are presented as the mean ± SEM. Statistical significance relative to *Prtg*^{+/+} is

indicated (*n* = 4 for each bar; * *p* < 0.05; ** *p* < 0.01; *** *p* < 0.001, by one-way ANOVA). **e** Western blot analysis of the *Prtg*, phosphorylated Smad2 (pSmad2), total Smad2, and Smad4 levels in *Prtg*^{+/+}, *Prtg*^{+/-}, and *Prtg*^{-/-} posterior trunk samples. Gapdh was used as an internal control. The molecular weight ladders are labeled, and the estimated molecular weight size is indicated by a tilde. **f** Quantitative results of (e). The level of pSmad2 was significantly decreased in the *Prtg*^{-/-} samples. Data are presented as the mean ± SEM. Statistical significance relative to *Prtg*^{+/+} is indicated (*n* = 4 for each bar; * *p* < 0.05; ** *p* < 0.01; *** *p* < 0.001, by one-way ANOVA).

signaling activity. Based on these findings, we hypothesized that *Prtg* regulates Gdf11 signaling activity to modulate pSmad2 levels. To test this hypothesis, we co-expressed *Prtg* and *Gdf11* in P19 embryonic carcinoma cells and accessed TGFβ signaling activity by using a CAGA-driven luciferase reporter. Our results showed that *Prtg* enhances Gdf11-mediated TGFβ signaling activity, whereas knockdown of *Prtg* (sh*Prtg*) led to reduced TGFβ signaling activity (Fig. 5a). In contrast, TGFβ signaling activity mediated by *Inhba* (activin A) or *Tgfb1* remained unaffected by *Prtg*. Furthermore, pSmad2 levels in cells expressing Gdf11 showed a significant correlation with expression levels of *Prtg* (Fig. 5b, c), indicating that *Prtg* specifically facilitates Gdf11-mediated TGFβ signaling.

Given that the expression of *Gdf11* was unchanged in *Prtg*^{-/-} embryos (Supplementary Fig. 3a and Supplementary Table 5), it is possible that *Prtg* regulates Gdf11 signaling activity through a post-translational mechanism.

Indeed, we demonstrated that *Prtg* interacts with Gdf11 in P19 cells by using co-immunoprecipitation, while no interaction was observed between *Prtg* and activin A (*Inhba*) or *Tgfb1* (Fig. 5d). Furthermore, we showed that the extracellular domain of *Prtg* is required for its interaction with Gdf11 (Fig. 5e, f). Using a TGFβ activity reporter assay, we found that the extracellular domain of *Prtg* (*Prtg* ET) alone was capable of facilitating Gdf11-mediated TGFβ signaling activity, whereas truncation of the extracellular domain (*Prtg* TC) completely abolished this ability (Fig. 5g). The levels of pSmad2 detected by western blot exhibited similar patterns as those observed with the TGFβ activity reporter assay (Fig. 5h, i). These results suggest that the extracellular domain of *Prtg*, but not the intracellular domain, is crucial for its interaction with and regulation of Gdf11 signaling activity. Taken together, our findings indicate that *Prtg* promotes Gdf11 signaling activity through protein-protein interaction.



Recapitulation of *Prtg*^{-/-} phenotypes in the hiPSC-derived PSM model

Our results from studying *Prtg*^{-/-} mice suggest that the vertebral transformation defect is caused by down-regulation of the Gdf11/Smad2 signaling activity and subsequent reduction of posterior *Hox* genes. To determine whether *Prtg* regulates posterior *Hox* gene expression via the Gdf11/

Smad2 signaling, we employed an in vitro model of axial and somite development derived from hiPSCs. Specifically, we adapted protocols from Lippmann, et al. and Matsuda, et al. to direct differentiation of hiPSCs into PSM through stepwise addition of activin A (ACT A), fibroblast growth factor 2 (FGF2), and CHIR99021 (a small-molecule agonist of the WNT/ β -catenin pathway) (Fig. 6a)^{26,40}. Over the course of 7 days, we observed a decrease in the

Fig. 4 | Decreased TGF β signaling activity in the PSM of *Prtg*^{-/-} embryos.
a Whole-mount immunostaining of *Prtg* (red), pSmad2 (green), and DAPI (blue) in E9.5 control and *Prtg*^{-/-} embryos. Digital transverse sections at the indicated levels in the whole-mount embryos are shown at the bottom ($n = 8$ embryos per group). Scale bars represent 500 μm . **b** Whole-mount immunostaining of *Hoxc10* (green) and DAPI (blue) in E9.5 control and *Prtg*^{-/-} embryos ($n = 4$ embryos per group). Digital transverse sections at the indicated levels in the whole-mount embryos are shown at the bottom. Arrowheads indicate the PSM regions. Scale bars represent 500 μm . D dorsal, V ventral. **c–e** Whole-mount in situ hybridization of *Ski* ($n = 2$) (**c**), *Skil* ($n = 2$)

(**d**), and *Smurf1* ($n = 2$) (**e**) in E9.5 control and *Prtg*^{-/-} embryos. Dashed lines indicate regions where the expression levels are decreased in *Prtg*^{-/-} embryos. Scale bars represent 500 μm . **f, g** Whole-mount in situ hybridization of *Hoxc10* ($n = 2$) (**f**) and *Hoxd10* ($n = 2$) (**g**) in E9.5 embryos. Red dashed boxes indicate regions of reduced expression levels of the indicated gene in *Prtg*^{-/-} embryos. Dashed lines indicate the positions of sections in the right panels. Scale bars represent 500 μm in whole-mount images and 100 μm in sections. fb forelimb bud, h heart, lpm lateral plate mesoderm, nc notochord, np neural plate, nt neural tube, ov otic vesicle, pa1 1st pharyngeal arch, psm presomitic mesoderm, sm somitic mesoderm.

expression of a stem cell marker *POU5F1/OCT4* based on RT-qPCR and western blot analyses (Fig. 6b, c, h). Expressions of primitive streak (PS) markers *TBXT* and *MIXL1* were increased from day 1, followed by a decrease after day 2. Expressions of PSM markers *TBX6* and *MSGN1* were detectable from day 1 to day 7. The expression profile of these marker genes indicated a process of paraxial mesodermal differentiation: hiPSCs initially differentiate into PS cells on day 1 and subsequently progress into PSM-like lineage. To evaluate the capability of our in vitro-induced PSM-like cells to further differentiate into somitic mesoderm, we exposed them to a combination of SB431542 (a TGF β signaling inhibitor), LDN193189 (a BMP signaling inhibitor), PD173074 (an FGF signaling inhibitor), and XAV939 (a Wnt signaling inhibitor) for 2 days (Supplementary Fig. 5a). These cells differentiated into somitic mesoderm based on the expression of *MEOX1*, a somite marker (Supplementary Fig. 5b–f). Taken together, at each stage of our induction and differentiation protocol, expected markers according to studies in animal models were appropriately expressed⁴¹, confirming that our stepwise protocol recapitulated the developmental trajectory of the somitic mesoderm.

We further examined *PRTG* expression in our hiPSC-PSM model. *PRTG* was initially detected on day 2, reaching its peak on days 3 and 4, followed by a decline on day 5, as observed at levels of both transcript and protein (Fig. 6b, c, h). To validate the axial patterning using our hiPSC-PSM model, we generated *PRTG* knockout (*PRTG*^{KO}) hiPSC lines using the CRISPR/Cas9 method (Fig. 6d, e and Supplementary Figs. 6 and 7). All *PRTG*^{KO} hiPSC clones (A5, A7, E8, and F4) exhibited similar characteristics as WT cells (N2 and G2), displaying normal stem cell morphology, high alkaline phosphatase activity, and the pluripotent cell marker *OCT4* (Supplementary Fig. 8). Upon differentiation into PSM, the expression profiles of markers for different stages, including *POU5F1*, *TBXT*, *TBX6*, *MSGN1*, and *MEOX1*, were comparable between the control and *PRTG*^{KO} lines (Fig. 6h). In addition, flow cytometry and immunocytochemistry analyses on day 5 of hiPSC-PSM differentiation revealed that appropriately 85% of cells were *TBX6*-positive, with no significant difference in *TBX6*-positive ratio between clones (Supplementary Fig. 9). These results demonstrate that *PRTG*^{KO} hiPSCs undergo normal differentiation into PSM-like cells.

We assessed *HOX* gene expression in *PRTG*^{KO} cells using our iPSC-PSM differentiation protocol. In the hiPSC-PSM model, *HOX* gene expression followed a collinear pattern similar to that in embryonic development (Fig. 6h and Supplementary Fig. 10). Specifically, *HOXB1* (an anterior *HOX* gene) and *HOXB6* (a trunk *HOX* gene) exhibited increased expression on post-induction days 1 and 2, while the posterior *HOX* genes *HOXC9* and *HOXC10* displayed up-regulation after day 3. The more posterior *HOX* gene *HOXC11* remained silent until day 7. In *PRTG*^{KO} cells, we did observe a delay in posterior *HOX* gene expression. In WT clones, *HOXC9* and *HOXC10* were expressed on day 3, whereas in *PRTG*^{KO} cells, their expression became noticeable only after day 4. Importantly, we observed a significant decrease in the level of pSMAD2 on day 7 of differentiation in *PRTG*^{KO} hiPSC-PSM cells (Fig. 6f, g). These findings demonstrate that, akin to mouse embryonic development, *PRTG* deficiency in a human cell model leads to diminished TGF β signaling activity and delayed and/or reduced expression of posterior *HOX* genes.

GDF11/SMAD2 signaling acts downstream of *PRTG* in regulating the expression of posterior *HOX* genes

To determine whether enhancing TGF β signaling activity could rescue the expression of posterior *HOX* genes in *PRTG*^{KO} hiPSC-PSM cells, we

administrated recombinant human GDF11 to the culture medium from day 3 to day 5 to activate the TGF β signaling in these cells (Fig. 7a). GDF11 supplementation increased the level of pSMAD2 in *PRTG*^{KO} cells (Fig. 7b, c), suggesting an elevation of TGF β signaling activity. Notably, the expression of posterior *HOX* genes, including *HOXC10*, *HOXD10*, *HOXA11*, and *HOXC11*, was significantly up-regulated in *PRTG*^{KO} hiPSC-PSM cells upon GDF11 administration on day 5 (Fig. 7d). Additionally, inhibition of SMAD2 phosphorylation by SB431542 suppressed the expression of *HOXC10*, whereas the induction of SMAD2 phosphorylation by other TGF β ligands, such as activin A and TGF β 1, enhanced its expression (Supplementary Fig. 11). These results suggest that the induction of posterior *HOX* genes is mediated by the TGF β /SMAD2 pathway, and that restoring TGF β /SMAD2 signaling activity with GDF11 is sufficient to rescue the delayed expression of posterior *HOX* genes in *PRTG*-deficient iPSC-PSM cells. Together with the phenotypic analysis of *Prtg*^{-/-} embryos and data from P19 cells, we demonstrate that the GDF11/SMAD2 signaling acts downstream of *PRTG* in regulating posterior *HOX* gene expression, therefore modulating vertebral axial patterning.

Discussion

The spatial and temporal expression of *Hox* genes during early embryonic development subdivides the vertebral column into distinct regions. Several signaling pathways, including the Wnt and TGF β , are known to define the anterior, trunk, and posterior/tail *Hox* gene expression. In addition, other molecules such as *miR-196*, *Nr6a1*, and retinoic acid have been shown to influence *Hox* expression^{22,42,43}. However, many factors involved in the regulation of the *Hox* gene remain to be uncovered. Here, we highlight the role of *Prtg* in governing the trunk-to-tail transition of *Hox* gene expression (Fig. 8). In *Prtg*-deficient mice, we observed a reduction in the level of pSmad2 in the tail region of E9.5 embryos, leading to the delayed activation of *Hox10* and *Hox11*. Consequently, this delay resulted in the anterior homeotic transformation of the posterior thoracic vertebrae. Furthermore, we showed that *Prtg* interacts with Gdf11 and facilitates Gdf11-mediated TGF β signaling activity. To further investigate these effects, we established an in vitro hiPSC-derived PSM-like model and successfully recapitulated the reduction of pSMAD2 and delayed expression of *HOX10* and *HOX11* in *Prtg*^{-/-} mouse embryos by using *PRTG*^{KO} cells. Our results demonstrate that GDF11 addition effectively elevated the level of pSMAD2 and rescued the expression of posterior *HOX* genes in *PRTG*^{KO} hiPSC-PSM cells. These findings underscore the critical role of *PRTG* in the GDF11/SMAD2-mediated activation of posterior *HOX* genes.

The abundant expression of *Prtg* during early embryogenesis highlights its role in regulating developmental processes. Our study indicates that *Prtg* regulates Gdf11 signaling to control axial patterning of the somitic mesoderm. Interestingly, *Gdf11*-mutant mice display severe defects in the developmental process, including down-regulation of *T*, *Tbx6*, and *Msgn1*, which are genes associated with the mesodermal fate²¹. In contrast, in *Prtg*^{-/-} embryos, the expression of *T*, *Tbx6*, and *Msgn1* remains mostly unchanged, and no obvious morphological abnormalities on E9.5 to E11.0 were observed (Supplementary Fig. 4a and Supplementary Data 1). These results suggest that, despite of down-regulation of the Gdf11 signaling in *Prtg*^{-/-} embryos, it remains sufficient to support most developmental processes. However, the timing of trunk-to-tail *Hox* code transition, which may be sensitive to Gdf11 signaling activity, appears to be delayed.

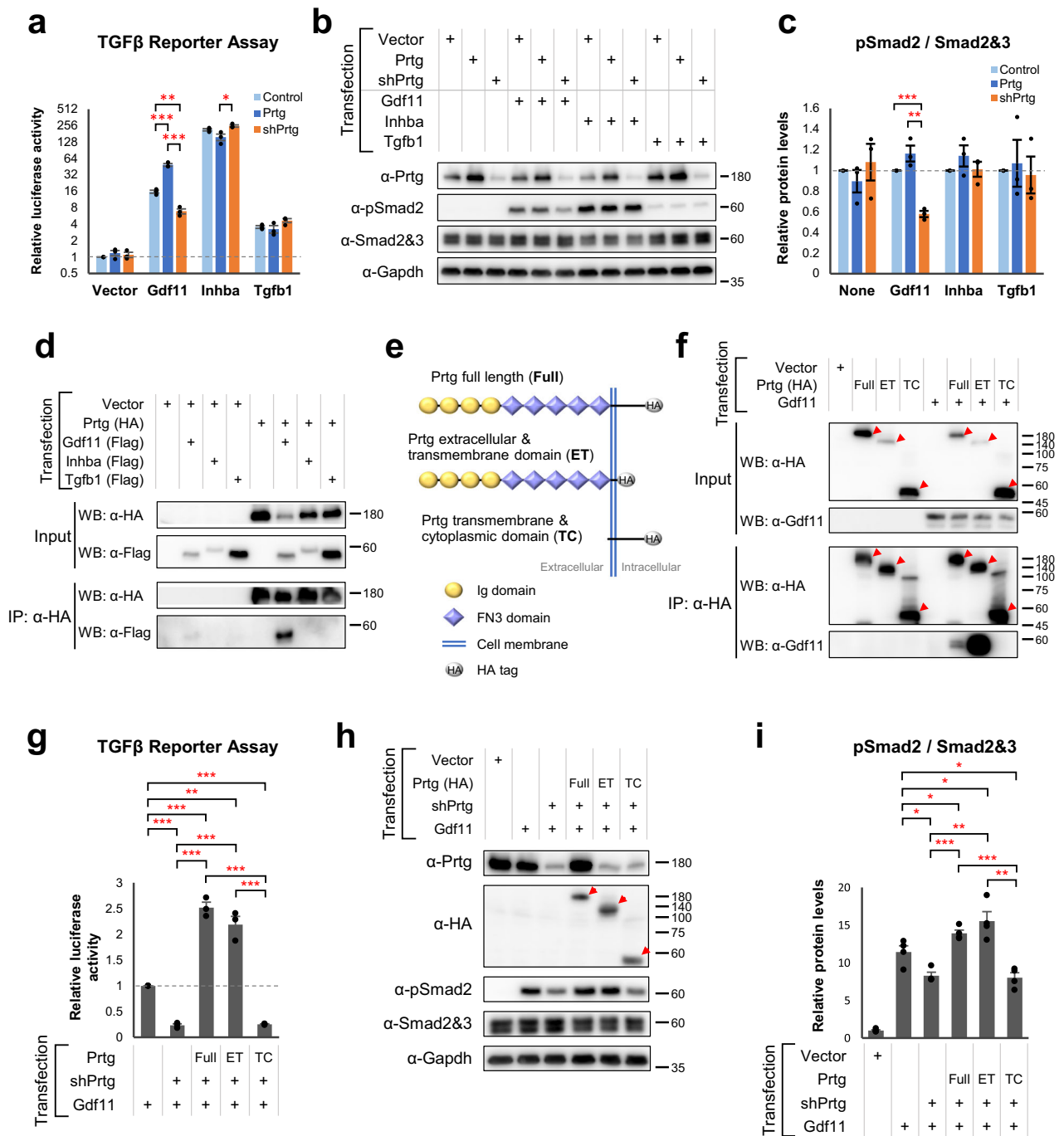
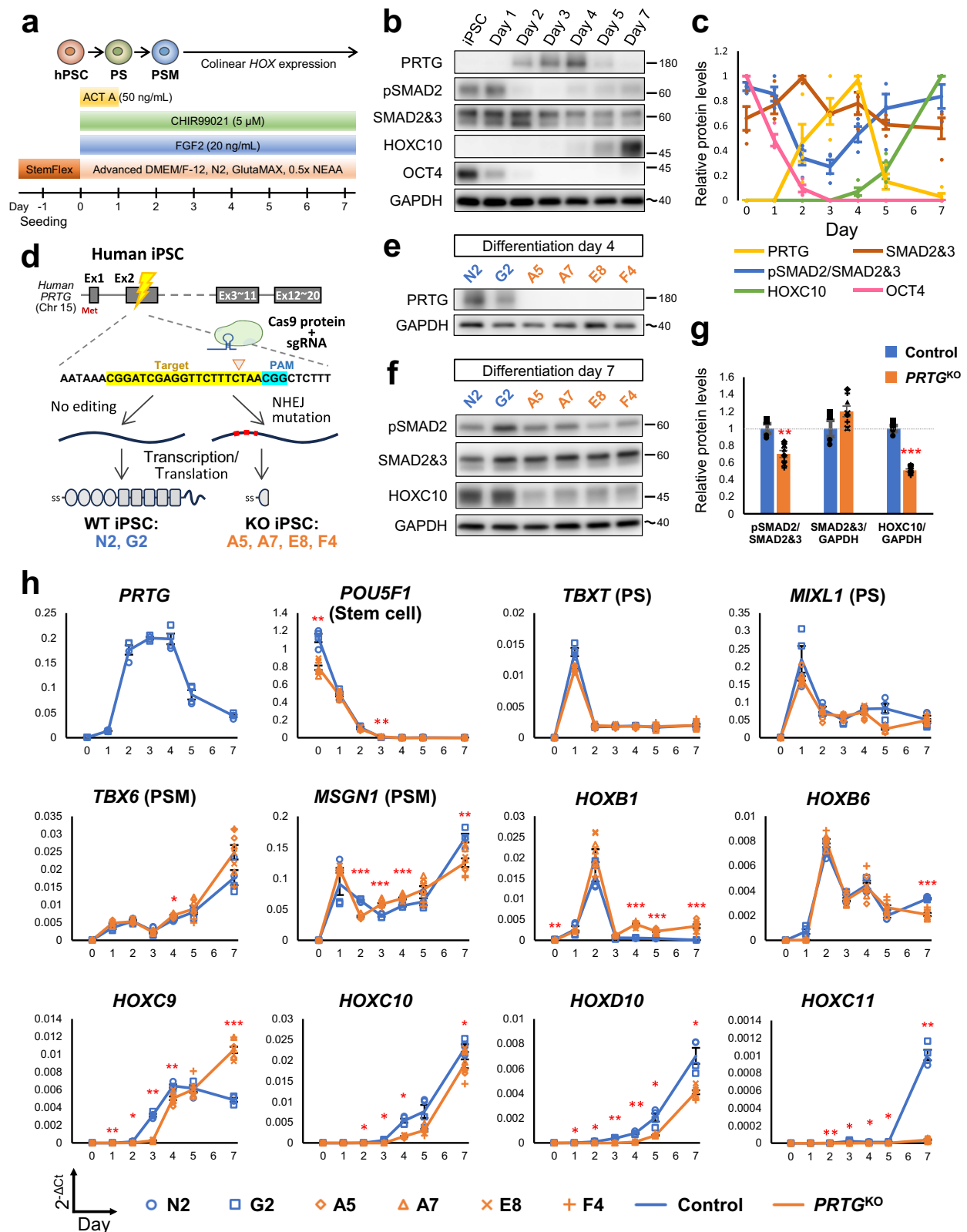


Fig. 5 | Prtg interacts with Gdf11 and modulates its signaling activity.

a (CAGA)₁₂-MLP-Luc reporter activities in P19 cells transfected with Gdf11, Inhba, Tgfb1, or a control, along with either *Prtg* overexpression or knockdown (shPrtg) vectors. Control and *Prtg* overexpression vectors contain a shRNA with a scrambled shPrtg sequence (shCtrl). Data are presented as the mean ± SEM. Statistical significance is indicated ($n = 3$ for each bar; * $p < 0.05$; ** $p < 0.01$; *** $p < 0.001$, by one-way ANOVA). **b** Protein levels of Prtg, pSmad2, and Smad2&3 were measured by western blot. Gapdh serves as an internal control. **c** Quantification of pSmad2 levels in **(b)**. Data are presented as the mean ± SEM. Statistical significance is indicated ($n = 3$ for each bar; * $p < 0.05$; ** $p < 0.01$; *** $p < 0.001$, by one-way ANOVA). **d** Co-immunoprecipitation of P19 cells transfected with HA-tagged Prtg and flag-tagged TGFβ ligands. IP immunoprecipitation, WB western blot. **e** Schematic illustration of

Prtg variants: full-length Prtg (Full), Prtg lacking the intracellular domain (ET), and Prtg lacking the extracellular domain (TC). **f** Co-immunoprecipitation of Prtg Full, Prtg ET, and Prtg TC with Gdf11 in P19 cells. Arrowheads indicate Prtg variants in the immunoblot images. **g** (CAGA)₁₂-MLP-Luc reporter activities in P19 cells expressing Gdf11 with Prtg Full, Prtg ET, or Prtg TC. Data are presented as the mean ± SEM. Statistical significance is indicated ($n = 3$ for each bar; * $p < 0.05$; ** $p < 0.01$; *** $p < 0.001$, by one-way ANOVA). **h** Levels of pSmad2 in P19 cells expressing Gdf11 with Prtg variants were analyzed by western blot. **i** Quantification of pSmad2 levels **(h)**. Data are presented as the mean ± SEM. Statistical significance is indicated ($n = 3$ for each bar; * $p < 0.05$; ** $p < 0.01$; *** $p < 0.001$, by one-way ANOVA).



The expression of *Prtg* shows a gradual decline in the tail region overall at E9.5 (Fig. 4a), although it remains highly expressed in the PSM of the tail. Notably, *Prtg* has also been found to be enriched in early NMPs compared with late NMPs⁴⁴, indicating that the level of *Prtg* is crucial during the trunk-to-tail transition. *Gdf11* and *miR-196*, both expressed in the tail region of the E9.5 embryo, synergistically suppress the trunk *Hox*

code in vitro²². Interestingly, embryos deficient for either *Gdf11* or *miR-196* show increased expression of *Prtg*^{21,43}, suggesting that *Prtg* is down-regulated by some posterior regulatory factors. Therefore, *Prtg* might initially function as an early stimulator of the *Gdf11* signaling to promote posterior fate, but is suppressed later following the activation of those posterior regulators.

Fig. 6 | Recapitulation of *PRTG* knockout (*PRTG*^{KO}) phenotypes observed in embryos using an in vitro hiPSC-derived PSM model. **a Schematic illustration of the differentiation protocol for generating induced pluripotent stem cell-derived presomitic mesoderm-like (iPSC-PSM) cells. PS, primitive streak; PSM, presomitic mesoderm. **b** The protein levels of *PRTG*, pSMAD2, SMAD2/3, HOXC10, and OCT4 at different time points in differentiated iPSC-PSM cells from control clones were measured using a western blot. The molecular weight of nearby ladders is labeled. The estimated molecular weight size is labeled using a tilde. **c** Quantification results of Fig. 5b. Data are presented as the mean ± SEM (*n* = 4). **d** Schema illustrating the generation of *PRTG*^{KO} (A5, A7, E8, and F4) and non-edited (G2 and N2) hiPSC clones via CRISPR/Cas9 gene editing. **e** *PRTG* expression in each hiPSC clone**

was validated using a western blot on day 4 of the iPSC-PSM model. **f** The protein levels of pSMAD2, SMAD2/3, and HOXC10 on day 7 of the hiPSC-PSM model were measured using a western blot. **g** Quantification results of Fig. 5f. Data are presented as the mean ± SEM (*n* = 4 for control group and *n* = 8 for *PRTG*^{KO} group) (***p* < 0.01; ****p* < 0.001; by student's *t*-test). **h** The expression levels of *PRTG*, stem cell marker (*POU5F1*, also known as *OCT4*), PS markers (*TBXT* and *MIXL1*), PSM markers (*TBX6* and *MSGN1*), *HOXB1*, *HOXB6*, *HOXC9*, *HOXD9*, *HOXC10*, *HOXD10*, and *HOXC11* from day 0 to day 7 of the differentiated hiPSC-PSM model were measured using RT-qPCR. *RPL13A* was used as the reference gene. Data are presented as the mean ± SEM (*n* = 4 for control group and *n* = 8 for the *PRTG*^{KO} group) (**p* < 0.05; ***p* < 0.01; ****p* < 0.001; by two-way ANOVA).

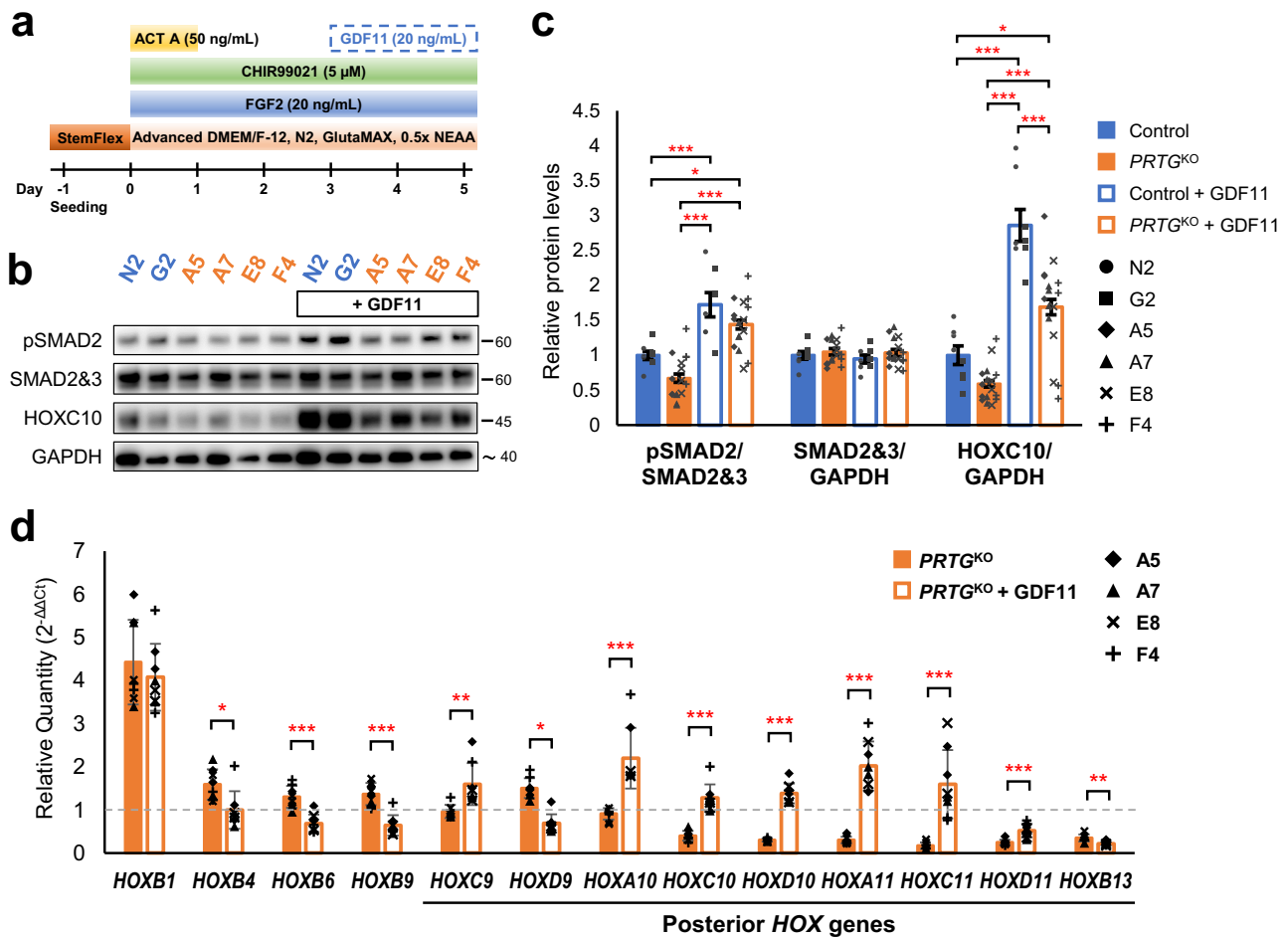


Fig. 7 | GDF11 administration rescues the delayed expression of posterior *HOX* genes in *PRTG*-deficient hiPSC-PSM cells. **a Schematic illustration of the experimental design. **b** Protein levels of pSMAD2, total SMAD2/3, and HOXC10 on day 5 of the *PRTG*^{KO} hiPSC-PSM model, with or without GDF11 treatment, were measured using western blot. **c** Quantification results of (b). Data are presented as the mean ± SEM (*n* = 8 in the control group and *n* = 16 in the *PRTG*^{KO} group; **p* < 0.05; ****p* < 0.001; by one-way ANOVA). **d** The expression levels of *HOXB1*, *HOXB4*,**

HOXB6, *HOXB9*, *HOXC9*, *HOXD9*, *HOXA10*, *HOXC10*, *HOXD10*, *HOXA11*, *HOXC11*, *HOXD11*, and *HOXB13* on day 5 of the *PRTG*^{KO} and GDF11-treated *PRTG*^{KO} iPSC-PSM cells were measured using RT-qPCR. *RPL13A* was used as the reference gene. Expression levels were normalized to the levels of control iPSC-PSM cells (N2 and G2 clones). Data are presented as the mean ± SEM (*n* = 8 in each group; **p* < 0.05; ***p* < 0.01; ****p* < 0.001; by student's *t*-test).

Our study suggests that *Prtg* plays a crucial role in promoting the transition of the trunk-to-tail *Hox* code by facilitating the *Gdf11*/*Smad2* signaling pathway. Although *Prtg* has not been previously reported to directly control the *Gdf11*/*Smad2* signaling in mammals, several studies have implicated the potential involvement of IgSF DCC subclass members in regulating the TGFβ pathway. For instance, in *Drosophila*, *Plum*, a distant homolog of *Prtg* and *Igdc4* (also known as *Nope*), promotes the signaling activity of myoglianin, the *Drosophila* homolog of *Mstn* and *Gdf11*⁴⁵. This regulation has been linked to axon pruning in the developing nervous system and synaptic function in the neuromuscular junction⁴⁶. Additionally,

WAP, follistatin/kazal, immunoglobulin, kunitz, and netrin domain containing 2 (*WFIKKN2*), a negative regulator of *Gdf11*, has been reported as a ligand for *Igdc3*, *Igdc4*, and *Prtg* in a recent study^{47,48}. These findings raise the possibility that regulation of the *Gdf11*/*Smad2* signaling by *Prtg* may involve additional molecules and have roles in other developmental processes, providing ways for future study.

We have demonstrated that *Prtg* regulates *Gdf11* through direct interaction, as validated by co-immunoprecipitation experiments showing that *Prtg* forms a protein complex with *Gdf11*. This interaction modulates *Gdf11*-mediated TGFβ signaling, consistent with our findings that *Prtg*

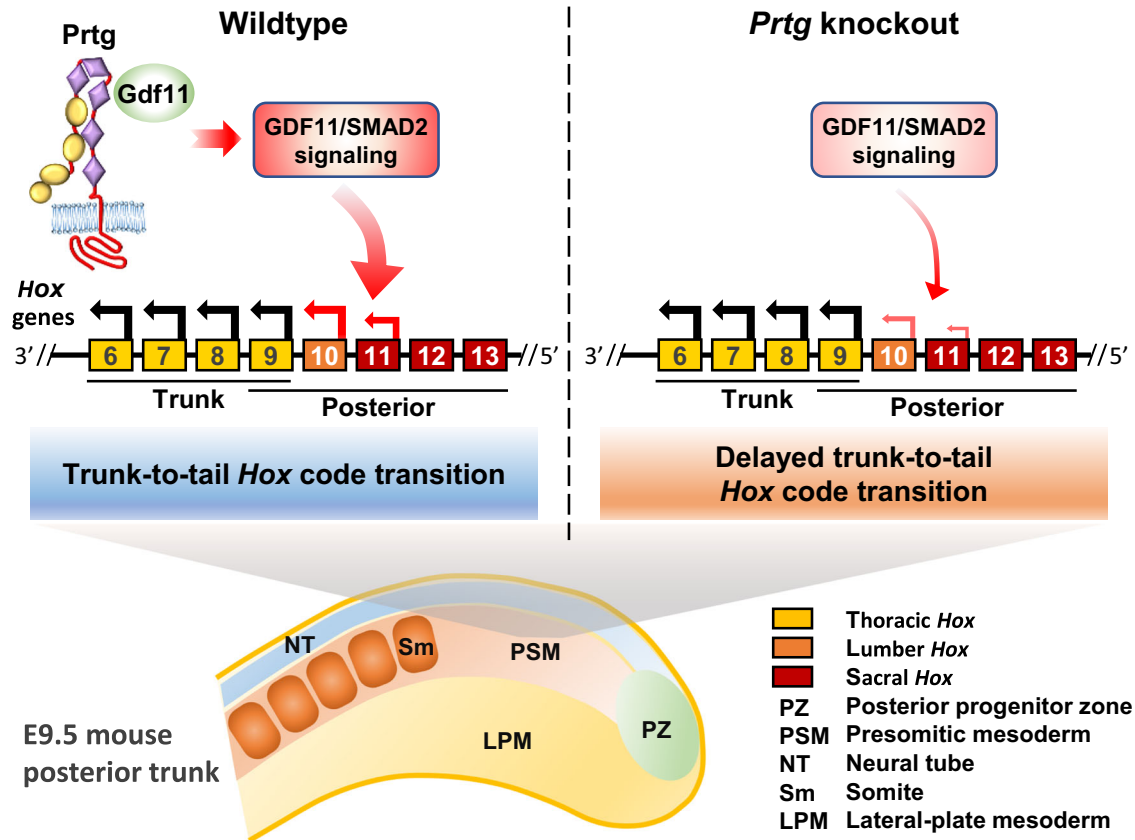


Fig. 8 | Delayed transition of thoracic-to-lumbar *Hox* code in *Prtg* knockout mice. A schematic representation illustrating the process of thoracic-to-lumbar *Hox* code transition in wild-type and *Prtg* knockout embryos. Arrows above the *Hox* genes denote the direction of *Hox* code translation. In wild-type mice, *Prtg* interacts with

Gdf11 to enhance TGFβ signaling, thereby facilitating the transition of the *Hox* code from thoracic to lumbar identity, which occurs in the tail region of E9.5 embryos. In *Prtg* knockout mice, decreased TGFβ signaling results in a delayed transition of the *Hox* code.

enhances the GDF11/pSMAD2 signaling in both embryos and the hiPSC-PSM cell model. Although *Prtg* interacts with Gdf11, it does not seem to function as a Gdf11 receptor, as the intracellular domain of *Prtg* does not have any known kinase activity and is not required for enhancing the Gdf11/pSmad2 signaling (Fig. 5). We propose that *Prtg* may function as a co-receptor within the Gdf11 signaling complex. Being present on the cell surface, *Prtg* could facilitate Gdf11 binding to its receptors, in a manner similar to how betaglycan enhances the binding of TGF-β2 to TGF-β receptors, or how Cripto enables Nodal binding to activin receptors and promotes Nodal signaling¹⁹. In addition, like other TGFβ ligands, Gdf11 is produced as a pro-peptide and requires proteolytic cleavage for activation¹⁹. Our results indicate that *Prtg* interacts with the Gdf11 pro-peptide, suggesting that *Prtg* may play a role in the proteolytic processing of Gdf11. Nevertheless, further investigation is needed to determine whether *Prtg* binds to Gdf11 receptors or participates in the proteolytic processing of Gdf11 to facilitate its signaling.

Another ligand of *Prtg*, Dnajb11 (also known as ERdj3), has been demonstrated to interact with *Prtg* to regulate neuronal differentiation²⁸. Our previous study also shows that interaction between *Prtg* and Radil affects integrin activation, which contributes to the regulation of migration and apoptosis in rostral cephalic neural crest cells³¹. Moreover, a recent study heightened *PRTG* expression in gastric cancer and *Helicobacter pylori*-infected tissues, with *PRTG* activation linked to cGMP/PKG axis stimulation, promoting the proliferation, metastasis, and chemoresistance of gastric cancer cells⁴⁹. Despite that *Prtg* is involved in various signaling pathways, whether these pathways participate in the regulation of *Prtg* on *Hox* gene expression or axial vertebral patterning has not been reported. Further investigation is required to determine whether these *Prtg*-modulated signaling pathways regulate *Hox* gene expression and axial vertebrate patterning during development.

The advantage of hiPSCs in reconstituting development *in vivo* has recently been evaluated. When cultured under defined conditions, hiPSCs differentiate into cell types such as NMPs, neurons, and somitic mesodermal cells^{26,40}. Their differentiation potential provides a relatively homogeneous sample for studying molecular mechanisms, thus simplifying the complicated condition *in vivo*. The hiPSC-derived organoids that form segment somite-like structures have recently raised the potential for modeling somitogenesis^{50–52}. However, in previous studies, these somite-like organoids did not fully activate the collinearity of *HOX* genes. Moreover, the expression of *HOXD10* and more posterior *HOX* genes was not detected, and the organoid failed to accomplish fully human somitogenesis. The defective development of the caudal body in these organoids closely resembles the phenotype in *Gdf11* mutant mice²¹. Interestingly, in our hiPSC-PSM model, *HOXD10* and even more posterior *Hox* genes were induced. Considering that the activation of posterior *HOX* genes requires GDF11/SMAD2 signaling activity, the gradual elevation of the pSMAD2 level in our hiPSC-PSM model after day 4 might have facilitated the expression of more posterior *HOX* genes. Indeed, GDF11 treatment has been used to trigger caudal *HOX* gene expression in studies that generated hiPSC-derived cells with regional identities²⁶. As the mechanism that activates endogenous *GDF11* expression during embryogenesis remains undiscovered, our hiPSC-PSM model potentially offers valuable insights into achieving complete somitogenesis.

In conclusion, our study provides evidence that *Prtg* interacts with Gdf11 and modulates Gdf11-mediated Smad2 activation in the developing paraxial mesoderm, thereby promoting posterior *Hox* gene expression and facilitating the trunk-to-tail transition during vertebral patterning. Our *in vitro* hiPSC-PSM model enables us to further investigate the molecular mechanism by which *PRTG* regulates GDF11 signaling activity. The roles of *PRTG*-mediated GDF11 signaling in other developmental processes, as well

as the mechanism by which this interaction facilitates GDF11/SMAD2 signaling activity, are key areas of interest for future research.

Methods

Animals and genotyping

The conventional *Prtg* knockout allele was generated as described previously³¹. All procedures involving mice were conducted in strict accordance with university guidelines. Ethical approval for animal experiments was obtained from the Institutional Animal Care and Use Committee of National Yang Ming Chiao Tung University (IACUC no. 1110111nr). For the genotyping of postnatal mice, tissue samples (a piece of the tail or foot finger) were lysed by incubating them with 300 μ L of 50 mM NaOH at 95 °C for 30 min, followed by neutralization with 50 μ L of 1 M Tris (pH 7.9). For embryo genotyping, the yolk sac was lysed in 30 μ L of 50 mM NaOH, heated at 95 °C for 30 min, and subsequently neutralized with 5 μ L of 1 M Tris (pH 7.9). Extracted DNA was subjected to PCR using Taq DNA polymerase (Geneaid) with the primer sequences listed in Supplementary Table 6.

Skeletal and cartilaginous tissue staining

Neonatal mice were euthanized, skinned, and eviscerated before staining. Cartilage was stained with Alcian Blue 8GX (Sigma-Aldrich) and skeletal tissue with Alizarin Red S (Sigma-Aldrich). Specimens were stored in 20% glycerol for photography. See Supplementary Methods for details.

Digoxigenin-labeled riboprobe synthesis

DNA templates were generated using high-fidelity PCR and subcloned into a pCRII-TOPO Vector (Invitrogen) or directly used for probe synthesis. Digoxigenin-labeled riboprobes were synthesized using T7 RNA polymerase (Roche) or SP6 RNA polymerase (Thermo Fisher Scientific) and purified using a Blood/Cell RNA Mini Kit (Geneaid). See supplementary methods for details. The primers used for probe preparation are listed in Supplementary Table 6.

Whole-mount in situ hybridization

Embryos were fixed in 4% paraformaldehyde (PFA)/phosphate-buffered saline (PBS) with 0.1% Tween 20 (PBST) overnight, dehydrated with methanol, rehydrated with PBST, bleached with 6% H₂O₂, and permeabilized with proteinase K (Roche). Digoxigenin-labeled riboprobes were used to probe target genes, and alkaline phosphatase-conjugated anti-digoxigenin Fab (Roche) was used to label the riboprobes. Color staining was performed using nitro blue tetrazolium (NBT, Sigma-Aldrich) and 5-bromo-4-chloro-3-indolyl-phosphate (BCIP, Sigma-Aldrich). See Supplementary Methods for details.

Total mRNA-seq and transcriptome analyses

Total RNA from E9.5 posterior tissues was purified using a Tissue Total RNA Mini Kit (Geneaid), and mRNA-seq was performed by GENEWIZ using an Illumina HiSeq sequencer. DEGs were generated using edgeR and analyzed via Qiagen IPA and GSEA. See Supplementary Methods for details.

RT-qPCR

Total RNA was extracted using the Tissue Total RNA Mini Kit (Geneaid) or Blood/Cell RNA Mini Kit (Geneaid), and genomic DNA was removed via on-column DNase digestion. SuperScript IV Reverse Transcriptase (Invitrogen) and anchored oligo dT(20)VN (Integrated DNA Technologies) were used to generate complementary DNA. RT-qPCR was performed using an ABI StepOnePlus instrument. TaqMan assays were performed using the PrimeTime Gene Expression Master Mix (Integrated DNA Technologies), and SYBR Green assays were performed using the PowerTrack SYBR Green Master Mix (Applied Biosystems). See Supplementary Methods for details. The sequences of the primers and probes are listed in Supplementary Table 6.

Western blot

Protein extracted from tissues or cells was cleaned by centrifugation, separated using sodium dodecyl sulfate–polyacrylamide gel electrophoresis, and transferred onto a polyvinylidene fluoride membrane (Millipore). The membrane was blocked with skimmed milk, probed using a primary antibody, and subsequently probed with horseradish peroxidase (HRP)-conjugated secondary antibody. A chemiluminescent HRP substrate was used for protein detection. See Supplementary Methods for details. The antibodies used for western blot are listed in Supplementary Table 7.

Whole-mount immunofluorescent staining

Embryos were collected using ice-cold PBS and fixed with 4% PFA/PBS for 4 h at 4 °C. Following fixation, the embryos were permeabilized using Tris-buffered saline (TBS) containing 1% Triton X-100, blocked with blocking buffer, and incubated with a primary antibody at 4 °C. The embryos were subsequently washed with blocking buffer and incubated with a secondary antibody overnight at 4 °C. Thereafter, they were cleaned with RapiClear (SunJin Lab) and imaged using a confocal microscope. See Supplementary Methods for details. The antibodies used for immunofluorescent staining are listed in Supplementary Table 7.

Vector construction

The mouse open reading frames of *Prtg*, *Gdf11*, *Inhba*, *Tgfb1*, and *Pcsk5* were amplified by PCR from the cDNA of E9.5–E10.5 mouse embryos and subsequently cloned into an expression vector derived from UI4-puro-SIBR. The DNA fragments containing either the *Prtg* knockdown sequence or its scramble control were cloned into the UI4-puro-SIBR, resulting in sh*Prtg* and shCtrl, respectively. All plasmids were verified by restriction enzyme mapping and Sanger sequencing. Primers and oligonucleotides used for cloning are listed in Supplementary Table 6. The constructed sequences with corresponding restriction enzyme sites are provided in Supplementary Data 2.

P19 cell culture and transfection

P19 embryonic carcinoma cells, purchased from Bioresource Collection and Research Center (BCRC Taiwan), were cultured in α -MEM (Gibco) supplemented with 10% FBS (Gibco) and 1 \times PSG (Gibco). Cells were passaged every two or three days when reached 80–90% confluence. During the passage, cells were rinsed with PBS, detached using TrypLE Express (Gibco), and reseeded on a new tissue culture dish. Transfection was performed using Lipofectamine 3000 (Invitrogen) according to the manufacturer's manual. See Supplementary Methods for details.

TGF β luciferase reporter assay

TGF β signaling activities were measured by a CAGA-driven luciferase reporter vector³³. Two days after transfection, cells were lysed in a passive lysis buffer (Promega), and luciferase activities were measured using the Dual-Luciferase Reporter Assay System (Promega). See Supplementary Methods for details.

Co-immunoprecipitation (Co-IP)

Two days after transfection, P19 cells were lysed in an IP lysis buffer. The lysates were clarified by centrifugation and incubated overnight with anti-HA antibody-conjugated resin. The resin was then washed three times with IP lysis buffer, and the protein complexes were extracted by heating in SDS sample buffer. See Supplementary Methods for details.

hiPSC culture

The hiPSC line NTUH-iPSC-02-02 (abbreviated as N2) was purchased from the Bioresource Collection and Research Center of the Food Industry Research and Development Institute, Taiwan. The use of these hiPSC lines followed the Policy Instructions of the Ethics of Human Embryo and Embryonic Stem Cell Research guidelines, in Taiwan. In addition, this study was approved by the institutional review boards of National Yang Ming Chiao Tung University (#YM110194W). Human iPSCs were routinely

maintained in StemFlex medium (Gibco) on vitronectin (VTN-N, Gibco) coated dishes at 37 °C in a 5% CO₂ incubator and passaged with ethylenediaminetetraacetic acid/Dulbecco's PBS according to the manufacturer's instructions. See supplementary methods for details.

Generation of *PRTG*^{KO} hiPSC lines using the CRISPR/Cas9 technique

DNA oligonucleotides for guide RNA (gRNA) targeting were designed using the TrueGuide CRISPR gRNA Design Tool (Thermo Fisher Scientific). The gRNA was complexed with the Cas9 protein (Invitrogen) and electroporated into hiPSCs. After recovery, individual colonies were expanded to establish isogenic cell lines. *PRTG* knockout in these cell lines was verified using western blot and confirmed via Sanger sequencing. See Supplementary Methods for details.

Induction of presomitic and somitic mesodermal cells

One day after cells were attached to a vitronectin-coated 24-well tissue culture plate, the medium was replaced with advanced Dulbecco's Modified Eagle Medium (DMEM)/F-12 (Gibco) containing 1× N-2 supplement (Gibco), 1× GlutaMAX supplement (Gibco), 0.5× non-essential amino acid (NEAA) supplement (Gibco), 50 ng/mL Activin A (PeproTech), 5 μM CHIR99021 (Tocris Bioscience), and 20 ng/mL FGF2 (PeproTech) to induce PS differentiation. For further PSM differentiation, the medium was exchanged with advanced DMEM/F-12 containing 1× N-2 supplement, 1× GlutaMAX, 0.5× NEAA, 5 μM CHIR99021, and 20 ng/mL FGF2. SM differentiation was then achieved by replacing the medium with advanced DMEM/F-12 containing 1× N-2 supplement, 1× GlutaMAX, 0.5× NEAA, 10 μM SB431542 (Tocris Bioscience), and 250 nM LDN193189 (Tocris Bioscience) for 1 day, followed by a final medium change to advanced DMEM/F-12 containing 1× N-2 supplement, 1× GlutaMAX, 0.5× NEAA, 1 μM XAV939 (Tocris Bioscience), and 100 nM PD173074 (Tocris Bioscience) for an additional day. See Supplementary Methods for details.

Immunofluorescence

hiPSCs were seeded on vitronectin-coated coverslips and subjected to iPSC-PSM differentiation. On day 5 of differentiation, cells were fixed with 4% PFA in PBS, permeabilized with methanol, blocked with 5% BSA in TBST, and incubated with primary antibodies overnight. The following day, coverslips were rinsed with TBST and incubated with secondary antibodies and DAPI. After staining, the coverslips were rinsed three times with TBST and mounted on slides with Fluoromount-G for imaging. See Supplementary Methods for details.

Flow cytometry

Day 5 hiPSC-PSM cells were detached with TrypLE and fixed with 4% PFA in PBS. Fixed cells were then permeabilized with methanol, blocked with 10% horse serum in TBST, and stained with primary and secondary antibodies. The stained cells were subsequently analyzed using a Beckman CytoFLEX S flow cytometer. See Supplementary Methods for details.

Statistics and reproducibility

Data are presented as means ± SEM. Statistical significance was assessed using a *t*-test, one-way ANOVA with Tukey testing, or two-way ANOVA with the original FDR method of Benjamini and Hochberg as a post hoc test. The *t*-test was conducted by Microsoft Excel. One-way ANOVA and two-way ANOVA were performed using GraphPad Prism software. Statistical significance is indicated in the figures as **p* < 0.05, ***p* < 0.01, and ****p* < 0.001. Each data point represents a single measurement or the mean of technical replicates from an embryo or sample collected from independently treated cells. The number of replicates is specified in the figure legends.

Reporting summary

Further information on research design is available in the Nature Portfolio Reporting Summary linked to this article.

Data availability

RNA-sequencing data are deposited in the NCBI database under accession number GSE256393. Uncropped blot images are provided in Supplementary Fig. 12. Constructed sequences generated in this study are listed in Supplementary Data 2. Source data underlying the graphs and charts in the main figures are included in Supplementary Data 3. All detailed experimental procedures are available in the Supplemental Information.

Received: 15 March 2024; Accepted: 29 November 2024;

Published online: 19 December 2024

References

- Mallo, M., Vinagre, T., & Carapuco, M. The road to the vertebral formula. *Int J. Dev. Biol.* **53**, 1469–1481 (2009).
- Martin, B. L. Mesoderm induction and patterning: insights from neuromesodermal progenitors. *Semin Cell Dev. Biol.* **127**, 37–45 (2022).
- Tzouanacou, E., Wegener, A., Wymeersch, F. J., Wilson, V. & Nicolas, J. F. Redefining the progression of lineage segregations during mammalian embryogenesis by clonal analysis. *Dev. Cell* **17**, 365–376 (2009).
- Henrique, D., Abranches, E., Verrier, L. & Storey, K. G. Neuromesodermal progenitors and the making of the spinal cord. *Development* **142**, 2864–2875 (2015).
- Hubaud, A. & Pourquie, O. Signalling dynamics in vertebrate segmentation. *Nat. Rev. Mol. Cell Biol.* **15**, 709–721 (2014).
- Scaal, M. Early development of the vertebral column. *Semin Cell Dev. Biol.* **49**, 83–91 (2016).
- Wellik, D. M. Hox patterning of the vertebrate axial skeleton. *Dev. Dyn.* **236**, 2454–2463 (2007).
- Holland, P. W. & Hogan, B. L. Expression of homeo box genes during mouse development: a review. *Genes Dev.* **2**, 773–782 (1988).
- McIntyre, D. C. et al. Hox patterning of the vertebrate rib cage. *Development* **134**, 2981–2989 (2007).
- Horan, G. S., Wu, K., Wolgemuth, D. J. & Behringer, R. R. Homeotic transformation of cervical vertebrae in Hoxa-4 mutant mice. *Proc. Natl. Acad. Sci. USA* **91**, 12644–12648 (1994).
- Horan, G. S. et al. Compound mutants for the paralogous hoxa-4, hoxb-4, and hoxd-4 genes show more complete homeotic transformations and a dose-dependent increase in the number of vertebrae transformed. *Genes Dev.* **9**, 1667–1677 (1995).
- Wellik, D. M. & Capecchi, M. R. Hox10 and Hox11 genes are required to globally pattern the mammalian skeleton. *Science* **301**, 363–367 (2003).
- Neijts, R. et al. Polarized regulatory landscape and Wnt responsiveness underlie Hox activation in embryos. *Genes Dev.* **30**, 1937–1942 (2016).
- Mazzoni, E. O. et al. Saltatory remodeling of Hox chromatin in response to rostrocaudal patterning signals. *Nat. Neurosci.* **16**, 1191–1198 (2013).
- Neijts, R., Amin, S., van Rooijen, C. & Deschamps, J. Cdx is crucial for the timing mechanism driving colinear Hox activation and defines a trunk segment in the Hox cluster topology. *Dev. Biol.* **422**, 146–154 (2017).
- McPherron, A. C., Lawler, A. M. & Lee, S. J. Regulation of anterior/posterior patterning of the axial skeleton by growth/differentiation factor 11. *Nat. Genet.* **22**, 260–264 (1999).
- Suh, J. et al. Growth differentiation factor 11 locally controls anterior–posterior patterning of the axial skeleton. *J. Cell Physiol.* **234**, 23360–23368 (2019).
- Wymeersch, F. J., Wilson, V., & Tsakiridis, A. Understanding axial progenitor biology in vivo and in vitro. *Development* **148**, dev180612 (2021).
- Derynck, R. & Budi, E. H. Specificity, versatility, and control of TGF-beta family signaling. *Sci. Signal.* **12**, eaav5183 (2019).

20. Tzavlaki, K. & Moustakas, A. TGF- β signaling. *Biomolecules* **10**, 487 (2020).
21. Aires, R. et al. Tail bud progenitor activity relies on a network comprising Gdf11, Lin28, and Hox13 genes. *Dev. Cell* **48**, 383–395 e388 (2019).
22. Hauswirth, G. M. et al. Breaking constraint of mammalian axial formulae. *Nat. Commun.* **13**, 243 (2022).
23. Gaunt, S. J., George, M. & Paul, Y. L. Direct activation of a mouse Hoxd11 axial expression enhancer by Gdf11/Smad signalling. *Dev. Biol.* **383**, 52–60 (2013).
24. Gaunt, S. J. Gdf11/Smad signalling and Cdx proteins cooperate to activate the Hoxc8 early enhancer in HepG2 cells. *Int J. Dev. Biol.* **61**, 427–432 (2017).
25. Mouilleau, V. et al. Dynamic extrinsic pacing of the HOX clock in human axial progenitors controls motor neuron subtype specification. *Development* **148**, dev194514 (2021).
26. Lippmann, E. S. et al. Deterministic HOX patterning in human pluripotent stem cell-derived neuroectoderm. *Stem Cell Rep.* **4**, 632–644 (2015).
27. Toyoda, R., Nakamura, H. & Watanabe, Y. Identification of protogenin, a novel immunoglobulin superfamily gene expressed during early chick embryogenesis. *Gene Expr. Patterns* **5**, 778–785 (2005).
28. Wong, Y. H. et al. Protogenin defines a transition stage during embryonic neurogenesis and prevents precocious neuronal differentiation. *J. Neurosci.* **30**, 4428–4439 (2010).
29. Vesque, C., Anselme, I., Couve, E., Chamay, P. & Schneider-Maunoury, S. Cloning of vertebrate protogenin (Prtg) and comparative expression analysis during axis elongation. *Dev. Dyn.* **235**, 2836–2844 (2006).
30. Takahashi, K. F. et al. Protogenin, a new member of the immunoglobulin superfamily, is implicated in the development of the mouse lower first molar. *BMC Dev. Biol.* **10**, 115 (2010).
31. Wang, Y. C. et al. Protogenin prevents premature apoptosis of rostral cephalic neural crest cells by activating the $\alpha 5 \beta 1$ -integrin. *Cell Death Dis.* **4**, e651 (2013).
32. Visvanathan, A. et al. Early rhombic lip Protogenin(+ve) stem cells in a human-specific neurovascular niche initiate and maintain group 3 medulloblastoma. *Cell* **187**, 4733–4750.e4726 (2024).
33. Nakao, A. et al. TGF- β receptor-mediated signalling through Smad2, Smad3 and Smad4. *EMBO J.* **16**, 5353–5362 (1997).
34. Whitman, M. Nodal signaling in early vertebrate embryos: themes and variations. *Dev. Cell* **1**, 605–617 (2001).
35. Lee, Y. J. et al. Growth differentiation factor 11 signaling controls retinoic acid activity for axial vertebral development. *Dev. Biol.* **347**, 195–203 (2010).
36. Oh, S. P. et al. Activin type IIA and IIB receptors mediate Gdf11 signaling in axial vertebral patterning. *Genes Dev.* **16**, 2749–2754 (2002).
37. Nakashima, M., Toyono, T., Akamine, A. & Joyner, A. Expression of growth/differentiation factor 11, a new member of the BMP/TGF β superfamily during mouse embryogenesis. *Mech. Dev.* **80**, 185–189 (1999).
38. Azhar, M. et al. Transforming growth factor β in cardiovascular development and function. *Cytokine Growth Factor Rev.* **14**, 391–407 (2003).
39. Jurberg, A. D., Aires, R., Varela-Lasheras, I., Novoa, A. & Mallo, M. Switching axial progenitors from producing trunk to tail tissues in vertebrate embryos. *Dev. Cell* **25**, 451–462 (2013).
40. Matsuda, M. et al. Recapitulating the human segmentation clock with pluripotent stem cells. *Nature* **580**, 124–129 (2020).
41. Tani, S., Chung, U. I., Ohba, S. & Hojo, H. Understanding paraxial mesoderm development and sclerotome specification for skeletal repair. *Exp. Mol. Med.* **52**, 1166–1177 (2020).
42. Chang, Y. C. et al. Nr6a1 controls Hox expression dynamics and is a master regulator of vertebrate trunk development. *Nat. Commun.* **13**, 7766 (2022).
43. Wong, S. F. et al. Independent regulation of vertebral number and vertebral identity by microRNA-196 paralogs. *Proc. Natl. Acad. Sci. USA* **112**, E4884–E4893 (2015).
44. Gouti, M. et al. A gene regulatory network balances neural and mesoderm specification during vertebrate trunk development. *Dev. Cell* **41**, 243–261.e247 (2017).
45. Yu, X. M. et al. Plum, an immunoglobulin superfamily protein, regulates axon pruning by facilitating TGF- β signaling. *Neuron* **78**, 456–468 (2013).
46. Sahota, V. K. et al. Plum modulates myoglianin and regulates synaptic function in *D. melanogaster*. *Open Biol.* **13**, 230171 (2023).
47. Kondas, K., Szlama, G., Nagy, A., Trexler, M. & Patthy, L. Biological functions of the WAP domain-containing multidomain proteins WFIKKN1 and WFIKKN2. *Biochem Soc. Trans.* **39**, 1416–1420 (2011).
48. Nickerson, K. R. et al. WFIKKN2 is a bifunctional axon guidance cue that signals through divergent DCC family receptors. Preprint at *bioRxiv* <https://doi.org/10.1101/2023.06.15.544950> (2023).
49. Xiang, T. et al. The novel ZEB1-upregulated protein PRTG induced by *Helicobacter pylori* infection promotes gastric carcinogenesis through the cGMP/PKG signaling pathway. *Cell Death Dis.* **12**, 150 (2021).
50. Sanaki-Matsumiya, M. et al. Periodic formation of epithelial somites from human pluripotent stem cells. *Nat. Commun.* **13**, 2325 (2022).
51. Miao, Y. et al. Reconstruction and deconstruction of human somitogenesis in vitro. *Nature* **614**, 500–508 (2023).
52. Yamanaka, Y. et al. Reconstituting human somitogenesis in vitro. *Nature* **614**, 509–520 (2023).
53. Itoh, S. et al. Direct binding of Smad3 and Smad4 to critical TGF β -inducible elements in the promoter of human plasminogen activator inhibitor-type 1 gene. *EMBO J.* **17**, 3091–3100 (1998).

Acknowledgements

The authors acknowledge Dr. David Turner for providing the vectors US2-puro, UI4-puro-SIBR, UI4-GFP-SIBR, and pRL-US2, as well as the National Genomics Center for Clinical and Biotechnological Applications of the National Core Facility for Biopharmaceuticals (NCFB), National Science and Technology Council (NSTC, Taiwan) for sequencing services. We also thank the Human Disease iPSC Service Consortium funded by the NSTC (112-2740-B-001-004) for iPSC generation and technical support. This work was financially supported by the Brain Research Center of National Yang Ming Chiao Tung University from the featured areas research center program within the framework of the Higher Education Sprout Project by the Ministry of Education (MOE) in Taiwan, and by NSTC grants to J.-Y.Y. (NSTC 112-2311-B-A49-003) and to Y.-H.W. (NSTC 111-2320-B-A49-027 and NSTC 113-2628-B-A49-015-MY3).

Author contributions

Conceptualization: Y.-S.H. and Y.-H.W. Experimentation and data analysis: Y.-S.H., W.-M.L., Y.-C.W., W.-C.K., and Y.-Y.C. Research supervision: M.-J.F., J.-Y.Y., and Y.-H.W. Manuscript preparation: Y.-S.H., J.-Y.Y., and Y.-H.W. Funding acquisition: M.-J.F., J.-Y.Y., and Y.-H.W. All authors discussed the results, provided feedback, and approved the final manuscript.

Competing interests

The authors declare no competing interests.

Additional information

Supplementary information The online version contains supplementary material available at <https://doi.org/10.1038/s42003-024-07342-8>.

Correspondence and requests for materials should be addressed to Jenn-Yah Yu or Yu-Hui Wong.

Peer review information *Communications Biology* thanks Amon Dias Jurberg and the other, anonymous, reviewer(s) for their contribution to the peer review of this work. Primary Handling Editors: Edwina McGlenn and Dario Ummarino.

Reprints and permissions information is available at <http://www.nature.com/reprints>

Publisher's note Springer Nature remains neutral with regard to jurisdictional claims in published maps and institutional affiliations.

Open Access This article is licensed under a Creative Commons Attribution-NonCommercial-NoDerivatives 4.0 International License, which permits any non-commercial use, sharing, distribution and reproduction in any medium or format, as long as you give appropriate credit to the original author(s) and the source, provide a link to the Creative Commons licence, and indicate if you modified the licensed material. You do not have permission under this licence to share adapted material derived from this article or parts of it. The images or other third party material in this article are included in the article's Creative Commons licence, unless indicated otherwise in a credit line to the material. If material is not included in the article's Creative Commons licence and your intended use is not permitted by statutory regulation or exceeds the permitted use, you will need to obtain permission directly from the copyright holder. To view a copy of this licence, visit <http://creativecommons.org/licenses/by-nc-nd/4.0/>.

© The Author(s) 2024